SOFT MATERIALS DESIGN VIA SELF ASSEMBLY OF FUNCTIONALIZED

ICOSAHEDRAL PARTICLES

By

VIDYALAKSHMI CHOCKALINGAM MUTHUKUMAR

A thesis submitted to the

Graduate School-New Brunswick

Rutgers, the State University of New Jersey

in partial fulfillment of the requirements

for the degree of

Master of Science

Graduate Program in Chemical and Biochemical Engineering

written under the direction of

Meenakshi Dutt Ph. D.

and approved by

New Brunswick, New Jersey

May, 2014

ABSTRACT OF THE THESIS

Soft Materials Design via Self Assembly of Functionalized Icosahedral Particles

by VIDYALAKSHMI CHOCKALINGAM MUTHUKUMAR

Thesis Director:

MEENAKSHI DUTT Ph. D.

In this work we simulate self assembly of icosahedral building blocks using a coarse grained model of the icosahedral capsid of virus 1m1c. With significant advancements in site-directed functionalization of these macromolecules [1], we propose possible application of such self-assembled materials for drug delivery. While there have been some reports on organization of viral particles in solution through functionalization, exploiting this behaviour for obtaining well-ordered stoichiometric structures has not yet been explored. Our work is in well agreement with the earlier simulation studies of icosahedral gold nanocrystals, giving chain like patterns [5] and also broadly in agreement with the wet lab works of Finn, M.G. et. al., who have shown small predominantly chain-like aggregates with mannose-decorated Cowpea Mosaic Virus (CPMV) [22] and small two dimensional aggregates with oligonucleotide functionalization on the CPMV capsid [1].

To quantify the results of our Coarse Grained Molecular Dynamics Simulations I developed analysis routines in MATLAB using which we found the most preferable nearest neighbour distances (from the radial distribution function (RDF) calculations) for different lengths of the functional groups and under different implicit solvent conditions, and the most frequent coordination number for a virus particle (histogram plots further using the information from RDF).

Visual inspection suggests that our results most likely span the low temperature limits explored in the works of Finn, M.G. et al., and show a good degree of agreement with the experimental results in [1] at an annealing temperature of $4\degree$C. Our work also reveals the possibility of novel stoichiometric N-mer type aggregates which could be synthesized using these capsids with appropriate functionalization and solvent conditions.

Acknowlegements

I wrote this Masters thesis under the supervision of Dr. Meenakshi Dutt from Rutgers University in Piscataway, NJ.

Table of Contents

List of Tables

Table of Figures

Chapter 1

Introduction

Soft Materials Design via Self Assembly of Functionalized Icosahedral Particles

With advances in synthetic routes enabling manipulation of icosahedral viral capsids at the molecular level [1] and chemical synthesis of metallic nanocrystals, the like of icosahedral gold nanocrystals [2], the next stage would be to investigate bottom up materials design using these icosahedral building blocks. **In this work we aim to simulate the self-assembly of tethered icosahedral building blocks and our results suggest aggregation into n-mer type aggregates, short linear chains and two dimensional networks and clusters. We use the Molecular Dynamics simulation technique.**

Viral capsids, owing to their monodisperse morphology, stability, recognition of cell surface receptors, rapid replication rates and recent availability of manipulation and functionalization methods, would be ideal candidates for targeted drug delivery and could also have applications in tissue engineering. N-mer type assemblies can be used to deliver multiple drugs with complementary actions. Using tailored functional groups it is also possible to generate pH responsive aggregates for application in tumors. DNA directed self assembly is being used to effectively control aggregate morphology in bottom-up materials design [3]. M. G. Finn et al., functionalized CPMV coat proteins with oligonucleotides and observed self assembly into two and three dimensional arrays [4] at different temperatures.

Also as suggested in the work of Bilalbegović [5] , icosahedral gold nanocrystals can also be assembled into linear chains and two dimensional structures for prospective applications

in electronic devices[6], catalysis [7, 8], and in diagnostics [9, 10] owing to superior optical properties. Our model predicts assembly into extensively networked chains, short chains and clusters, and small two dimensional patterns emerging using different anisotropic functionalized icosahedral building blocks.
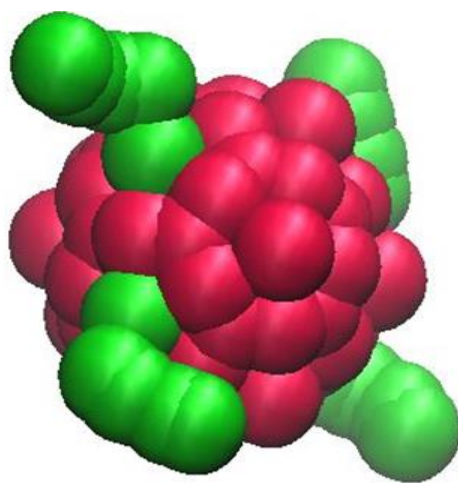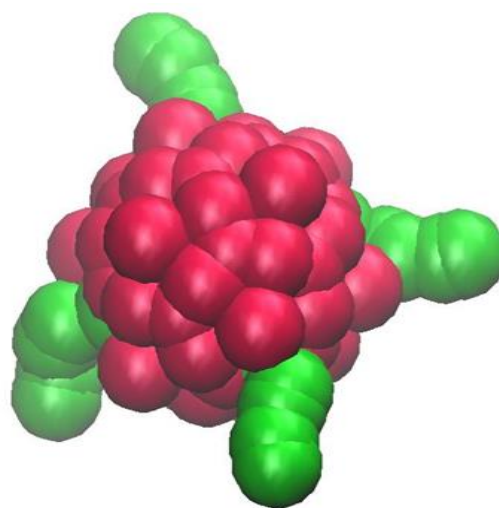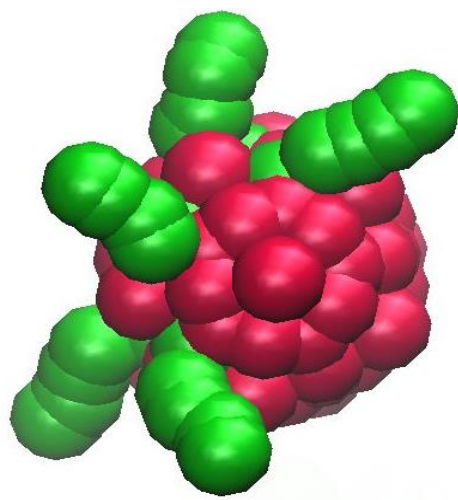
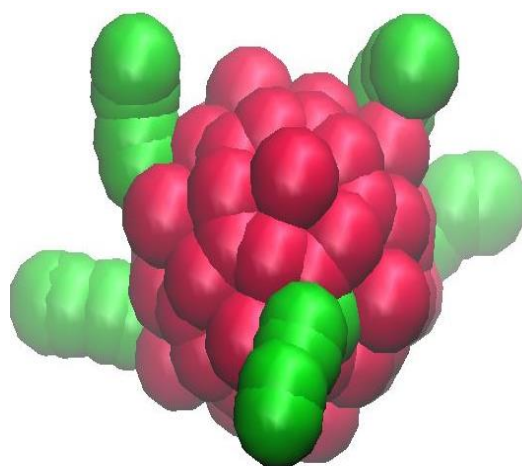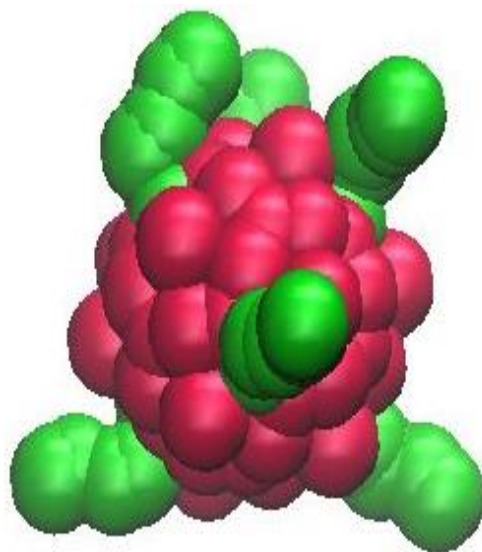**Figure 1)**
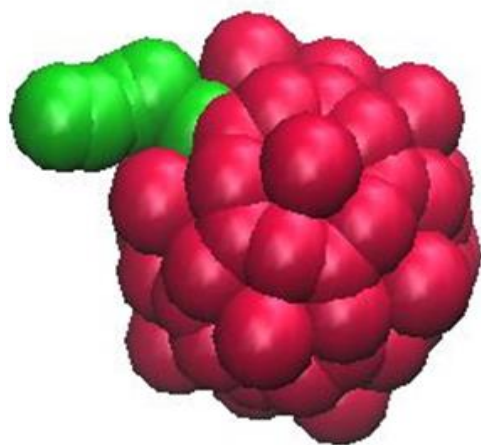

(1A)
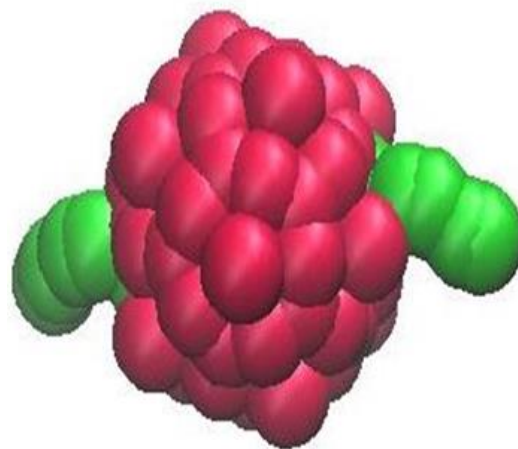
(1B)

(1C)

(1D)

(1E)

(1F)

(**1G**)

Figure 1) KEY:

A) Single tether; B) Two opposite tethers ; C) Four tethers, two on each side arranges as (B); D) Four tethers in a single plane spaced more symmetrically around the capsid; Five tethers forming corners of a rectangular pyramid E) All vertices on the same side of the capsid F) One vertex opposite to the other four vertices ; G) Six tethers at the outer most vertices of the capsid along 3D axes.

Figure 2)

Auxiliary cartoon:
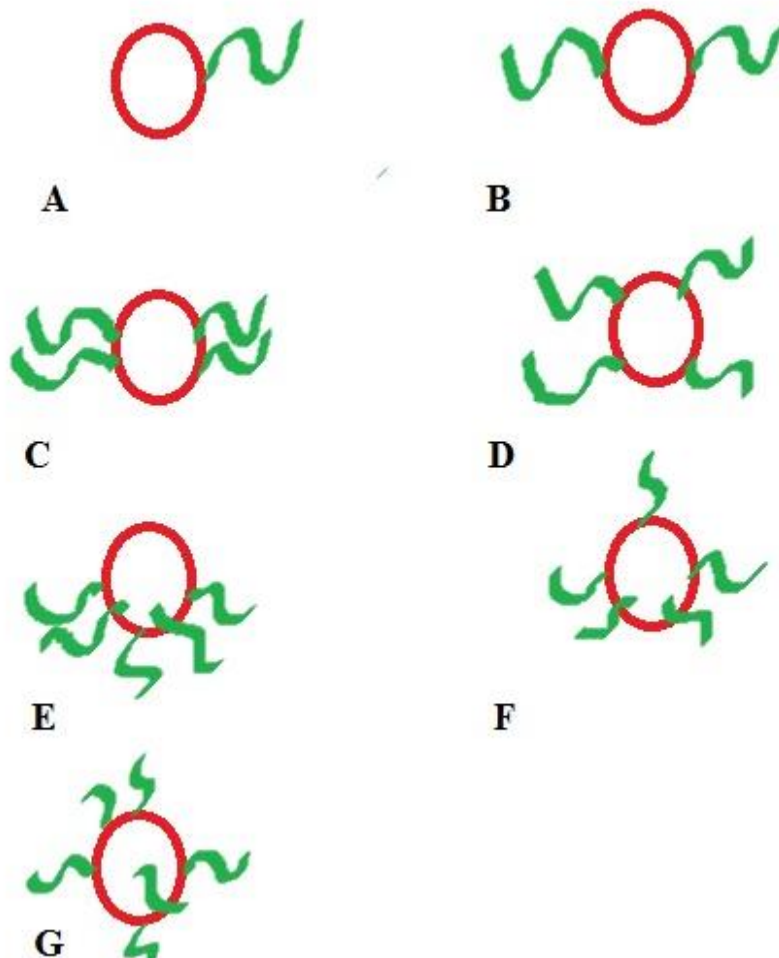
Chapter 2

Model and Methods

We model assembly dynamics using Molecular Dynamics (MD) simulation [11-13] with the LAMMPS [14] open source package. Equation of motion for each bead i is given by $\mathbf{F}_i = m_i\mathbf{a}_i$ where, F_i is the force acting on bead i, m_i is the mass of bead i and a_i is the acceleration of bead i. The force can be expressed as the gradient of the potential energy U by the relations $\mathbf{F}_i = -\nabla_i U$ with $U = U_{pair} + U_{bond}$, where U_{pair} and U_{bond} are the potential energies from all pair and bond interactions, respectively. The dynamics of each bead i is determined by the following equations $-\nabla_i U = m_i\mathbf{a}_i = m_i\frac{\partial^2\mathbf{r}_i}{\partial t^2} = m_i\frac{\partial\mathbf{v}_i}{\partial t}$ and $\mathbf{v}_i = \dot{\mathbf{r}}_i$, where $\mathbf{r}_i$ and $\mathbf{v}_i$ are the position and velocity vectors of bead i. The equations of motion will be integrated using the Velocity Verlet method [15] which has greater stability, time reversibility and preserves the symplectic form on the phase space compared to the Euler method [16]. The position $\mathbf{r}_i$ and velocity $\mathbf{v}_i$ of a bead i using the Velocity Verlet algorithm are calculated as follows: $\mathbf{v}_i(t+\Delta t) = \mathbf{v}_i(t) + \frac{1}{2}(\mathbf{a}_i(t) + \mathbf{a}_i(t+\Delta t))\Delta t$ and

$\mathbf{r}_i(t+\Delta t) = \mathbf{r}_i(t) + \mathbf{v}_i(t)\Delta t + \frac{1}{2}\mathbf{a}_i(t)\Delta t^2$, where $\mathbf{r}_i(t)$, $\mathbf{r}_i(t+\Delta t)$, $\mathbf{v}_i(t)$ and $\mathbf{v}_i(t+\Delta t)$ are respectively the position and velocity vectors at time t and $t+\Delta t$ (Δt is the integration time step.) The MD simulations will sample the canonical ensemble and will be run using the open source parallelized MD program called LAMMPS.We use ViperDB [17] atom information of 1m1c icosahedral cage to generate a 180-bead coarse grained model for the icosahedral nanoparticle, which is then

functionalized with 1, 2, 4, 5, or 6 tethers of 5, 10, 15 or 20 beads (Figure 1). The simulations are executed for 216 nanoparticles in cubic boxes with the number density of icosahedral building block varying from 0.002370 to 0.000064 corresponding to box dimensions of 45σ and 150σ respectively. As a measure of nanoparticle size, it can be noted that twice the radius of gyration of the nanoparticle is 3.744σ, while the size of a bead is 1.0 σBoth, the attractive and repulsive interactions in the system are modeled using 12-6 Lennard-Jones (LJ) potential [18-19] as below, with a cut off at 2.5σ and 1.0σ respectively.

$$E = 4 * \epsilon * \left[\left(\frac{\sigma}{r}\right)^{12} - \left(\frac{\sigma}{r}\right)^{6} \right]$$

The bonds between tether beads and connecting the nanoparticle and tether are modeled in the bead spring polymer FENE style as below,

$$E = 0.5 * K * R^2 * \ln\left[1 - \left(\frac{r}{R}\right)^2\right] + 4 * \epsilon * \left[\left(\frac{\sigma}{r}\right)^{12} - \left(\frac{\sigma}{r}\right)^{6}\right] + \epsilon$$

Where, K is in (energy/distance^2), R in (distance), epsilon in (energy), sigma in (distance).

We model two solvent conditions implicitly, favoring aggregation of nanoparticles over tethers (good solubility of tethers in the solvent) and vice-versa. The system is first equilibrated at a high temperature of 4.0 and then suddenly cooled to the desired temperature of 0.25 at which self assembly is studied, using the Langevin thermostat [20-22].

Analysis Routines: Methodology

Table 1: Simulation Parameters for Lammps (lj units)

Time-step for MD	0.001
K	30
R	1.5
ϵ	0.0
σ	0.0
Simulation box	Periodic boundary, cubic box
Langevin thermostat	0.25 temperature, 0.1 damping

1) Read final coordinate information from Lammps [14] output file.

2) Computed the coordinates for the center of mass (COM) for each nanoparticle (excluding tether beads).

3) Calculated distances between all possible pairs of COMs.

4) Divided the distance range by bin size of 0.5 units. Radial distribution function (RDF) plot is generated from this information using the following formula:

$$g(r) = \lim_{dr \to 0} \left[\frac{p(r)}{\left\{ 4 * \pi * \left(\frac{Npairs}{V} \right) * r^2 * dr \right\}} \right]$$

Where,

p(r) is the average number of atom pairs found at a distance between r and r+dr;

Npairs is the number of unique pairs of atoms. In our simulations it is a constant value of (216 X 215)/2;

And 'r' measures distance.

5) Same information was re-read to give information as the number of neighbors (defined by nearest neighbor distance from the RDF plots) for each COMs. This information was sorted to present the population plots.

6) Location of the peaks and area under the peaks for the RDF plots was also calculated.

Chapter 3

(3.1)Results and Discussion

We assess the properties of these mesoscopic assemblies using the radial distribution function plot and a histogram of probable coordination numbers for any given arrangement and interaction.

For generating the radial distribution function, we use the center of mass of the icosahedron and histogram,

$$g(r) = \lim_{dr \to 0} p(r)/(4 * \pi * (\frac{N}{V}) * r^2 * dr)$$

where r is the distance between a pair of particles, p(r) is the number of atom pairs found at a distance between r and r+dr after running the simulation for five million time steps with a given interaction potential, V is the total volume of the simulation box, and N is the total number of unique pairs of nanoparticles. The 'radius' in the radial distribution plot is scaled by the factor of 3.744, which is twice the radius of gyration of the naked icosahedron. As can be noted the nearest neighbor distance for all simulations lies between 4.5σ to 6.0σ. The first neighbor peak at 4.5σ is attributed to the deviation from the spherical geometry for which the equivalent dimension would only be 3.7441σ, while the occurrence of the first nearest neighbor at distances greater than 4.5 is due to the specific arrangement and size of tethers or the interaction potential in play.

The nearest neighbor histogram plots inform us the most probable coordination number of a particle in the box. And when coupled with the radial distribution function plot and visual inspection gives us clues to the preferred arrangement of nanoparticles in the box.
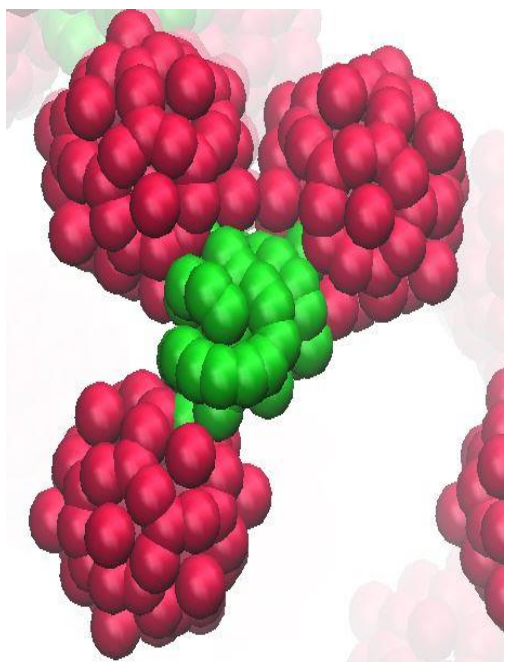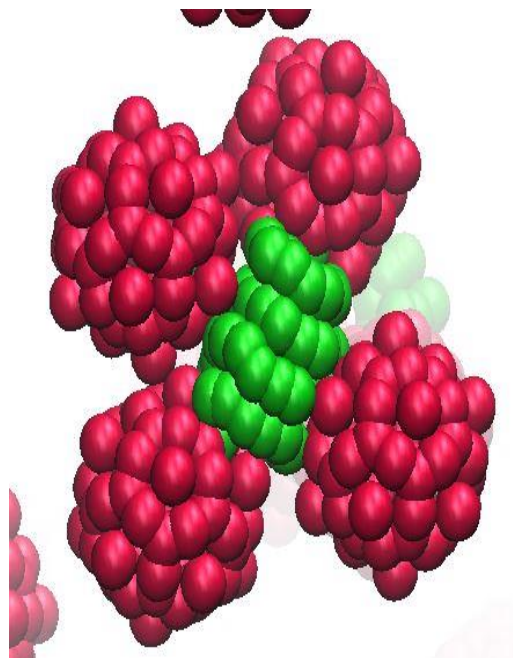
Chapter 3.2

N-mer type aggregates
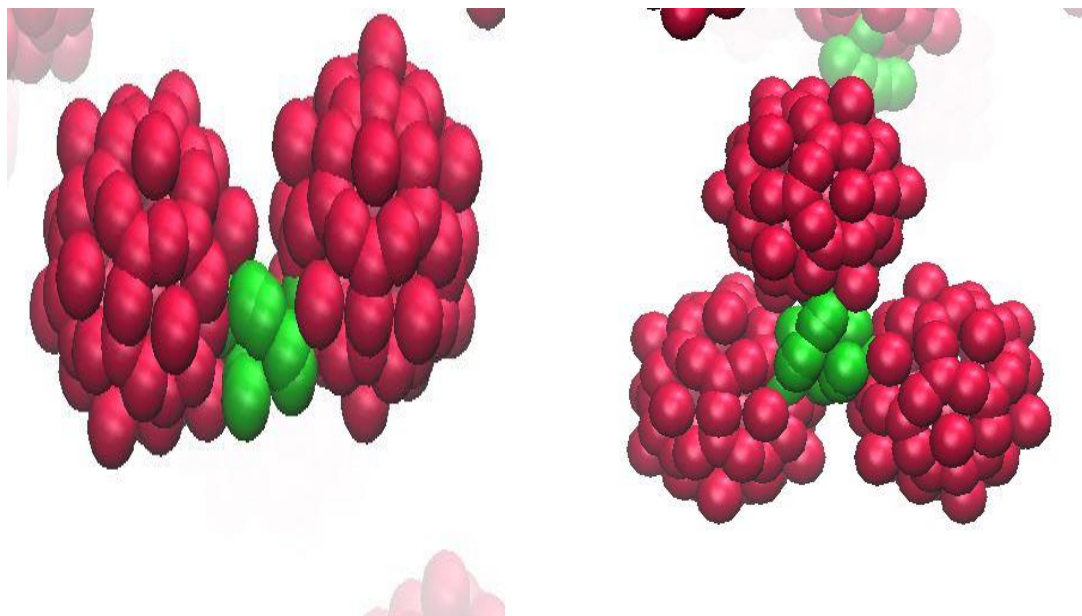
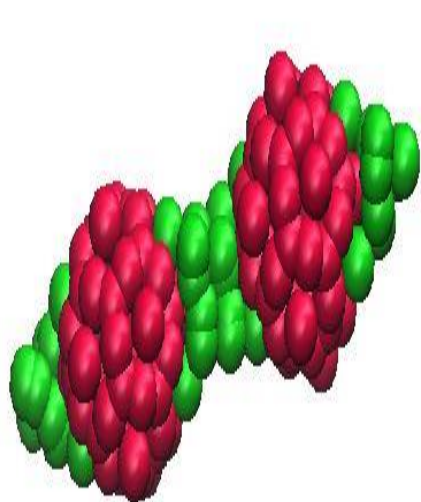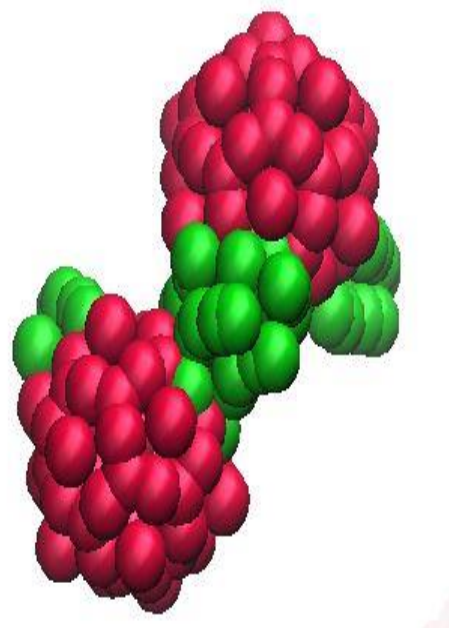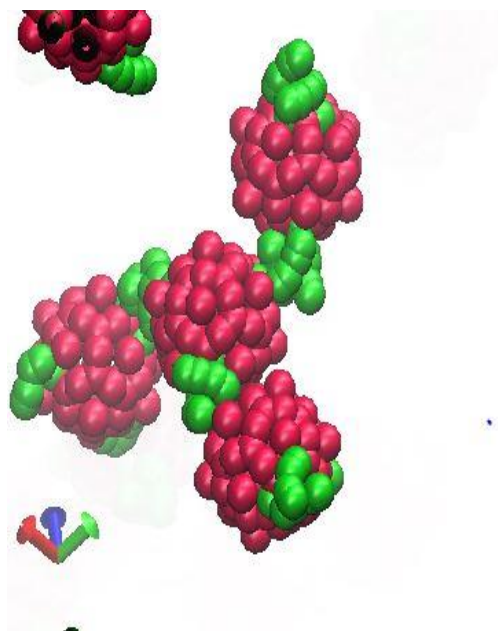**Figure 3)**

(3A)   (3B)
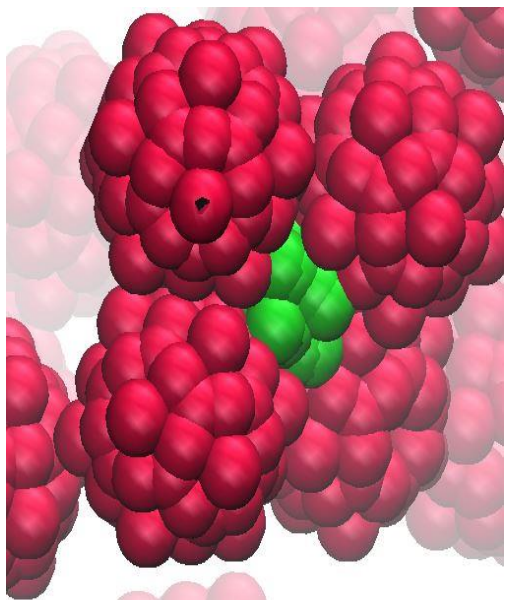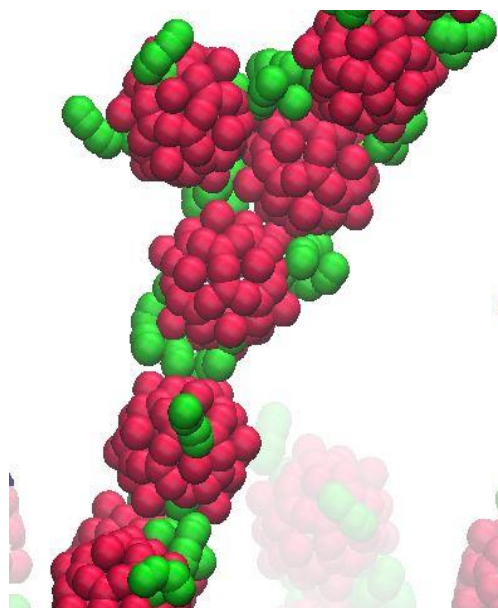
(3C)
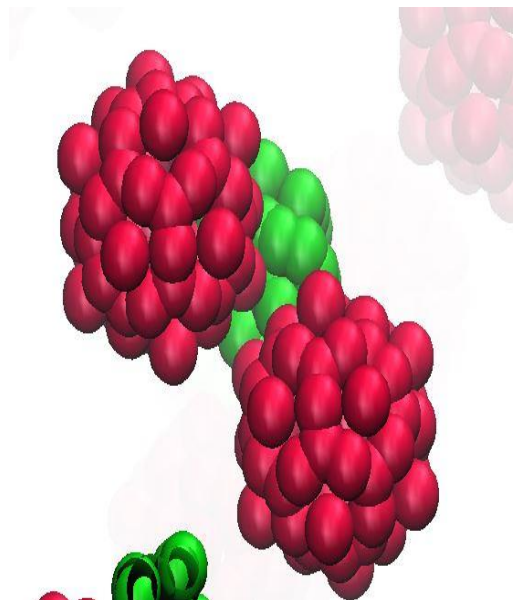
(3D)
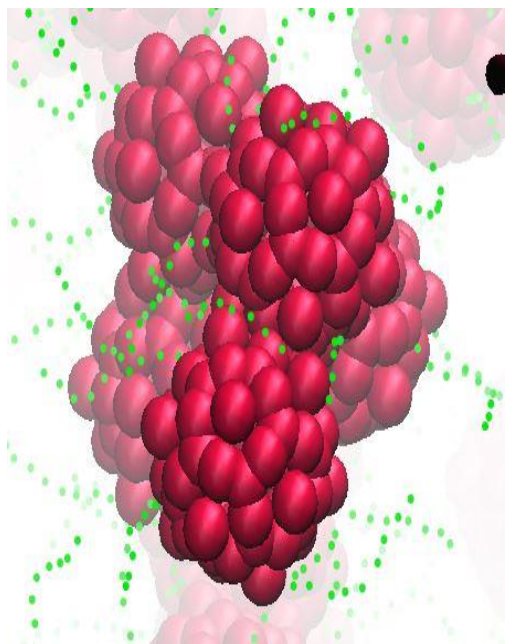
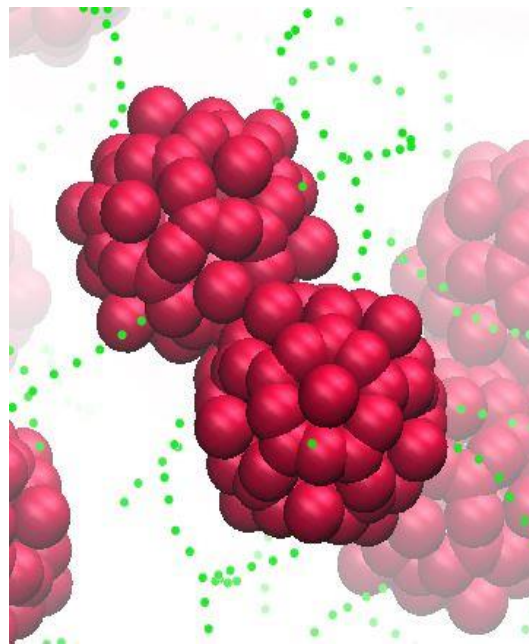

(3E)

(3F)

(3G)

(3H)

(3I)

(3J)

(3K)

(3L)
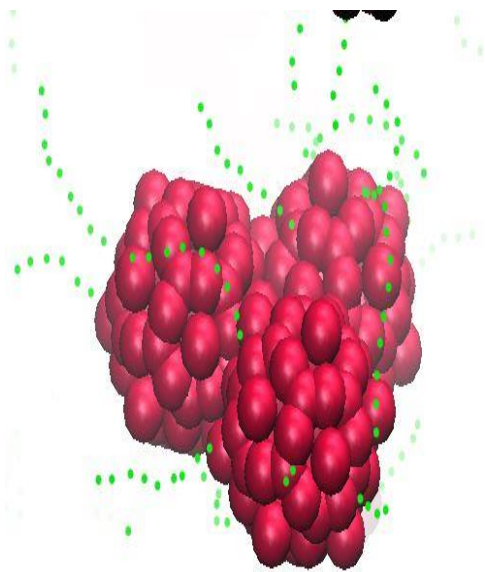
(3M)

Figure 3-Key

Figures A-K: Solvent conditions under which tethers aggregate

A) 5 beads, single functionalization, dimer

B) 5 beads, single functionalization, trimer

C) 5 beads, single functionalization, tetramer

D) 15 beads, single functionalization, chains attractive- dimer

E) 15 beads, single functionalization, trimer

F) 15 beads, single functionalization, tetramer

G) 5 beads, anisotropy 1C

H) 5 beads, anisotropy 1E

I) 5 beads, anisotropy 1G

J) 5 beads, anisotropy 1D

Figures (K-M): Solvent conditions under which capsids aggregate

K) 10 beads, 6 tethers, Box dimension 50σ, clusters

L) 10 beads, 6 tethers, Box dimension 50σ, dimer

M) 10 beads, 5 tethers of anisotropy 1E, Box dimension 50σ, trimer

We frequently observed n-mer type aggregates under solvent conditions favoring the aggregation of tethers. This type of aggregation was favored for all densities in the more anisotropic structures, 1A, 1E and 1F. And they also appeared in low density systems for other arrangements of tethers. The single tethered icosahedron in Figure 1A, for all tether lengths results in dimers, trimers and tetramers as captured in figures 3A-3F. Figure 4, shows the radial distribution function observed for this morphology 1A, at a density of 0.00079 nanoparticles per σ^3.

We found that these n-mer type aggregates can have coordinating neighbors at distances anywhere from 5.0-6.0, depending on the density and tether length. The first peak for systems with 5, 10 and 15 beads in the tether was observed to be at 5.0σ, corresponding to 1.33 units in the radial distribution plot. For the system with 20 beads in tether, it was observed that the first peak shifts to 5.5σ. The second peak appears at $6.0-6.5\sigma$ and becomes more prominent in systems with more number of beads in the system. As can be seen in figure(5), for the single functionalized system with 15 tether beads at a density of 0.00237, the fraction of trimers at 6.5σ is 28% while at 5.0σ it is only 15%. At a lower density of 0.00078, the fraction of dimers and trimers is still higher at 6.0σ (Figure 4, D) compared to 5.0σ (Figure 4, C). As these systems only formed N-mer type of aggregates and both these distances correspond to the directly coordinating neighbor, we generated histogram plot to observe the cumulative numbers of neighbors at any of these distance points. And the plot suggests that within aggregates both these coordinating distances can appear and thus, the histogram in figure 5(E) and 5(F) show several more trimers, tetramers and pentamers which could not be shown using the histogram for each of these distances separately. The increase in the fraction of uncoordinated atoms with the decrease in density

is also confirmed at both these distances. To calculate the number of aggregates of each type roughly, we can use the following relation:

Number of N-mers= (Fraction * 216)/N

While anisotropies in 1B and 1C result mostly in chains type aggregates, other anisotropies result in few N-mer type arrangements (Figures 3G-3J) but the confirmations are not regular and the probabilities of occurrence of chain like arrangements in these systems remains higher compared to N-mer type arrangements. This can be verified by the nearest neighbor histogram plots for these systems with higher probabilities of 2 nearest neighbors (Figure 6A-D) even for high density systems. From figures 6E-F, the fall in coordination numbers with decrease in density can also be deduced. The conditions favoring the aggregation of nanoparticles also result in chain like configurations with few N-mer type aggregates (Figure 3L-N) observed in simulation runs.

Figure 4)

4A) Beads 5
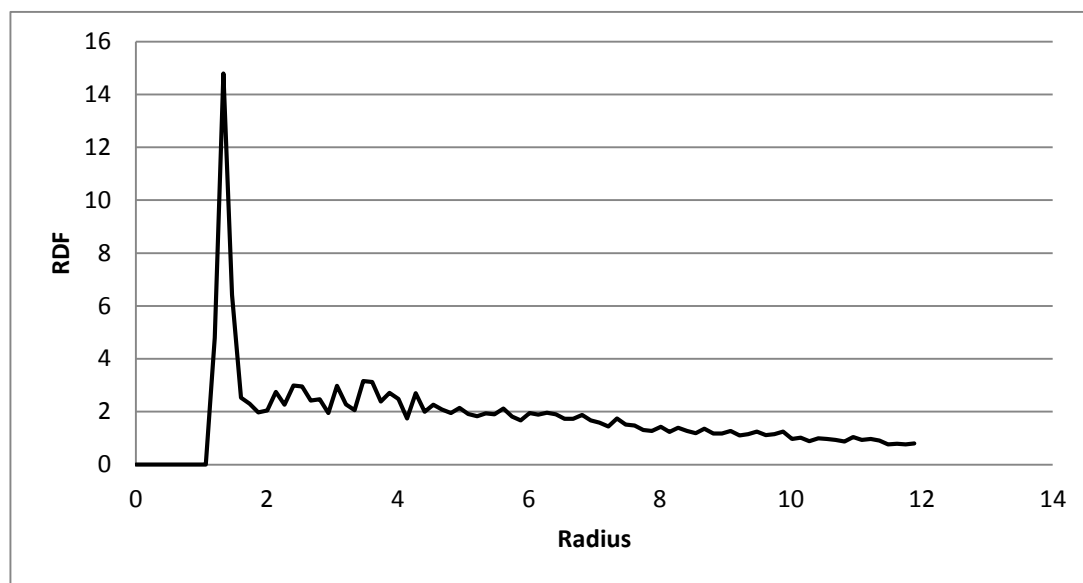
4B) Beads 10
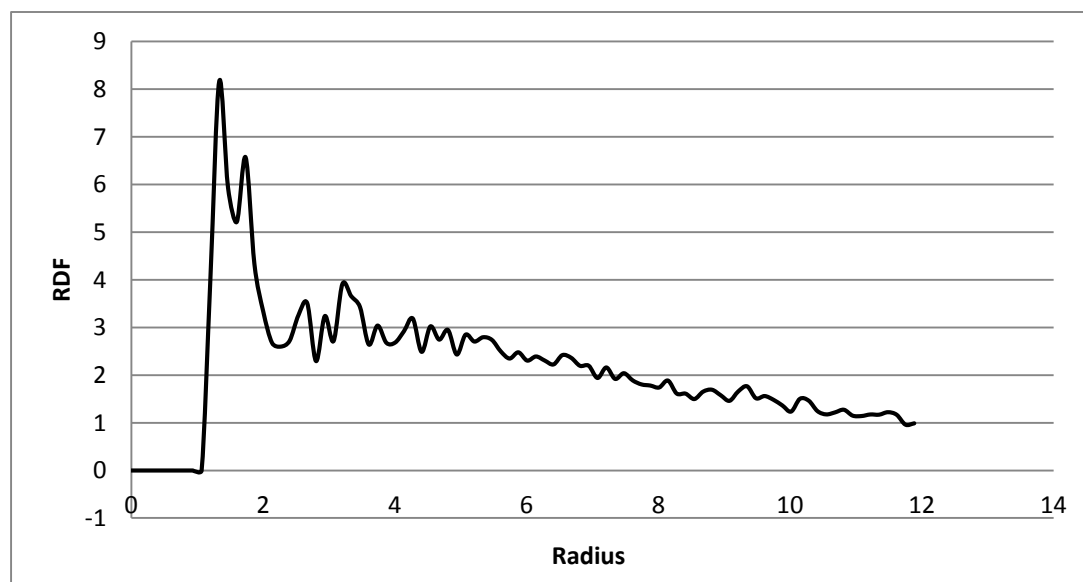
4C) Beads 15
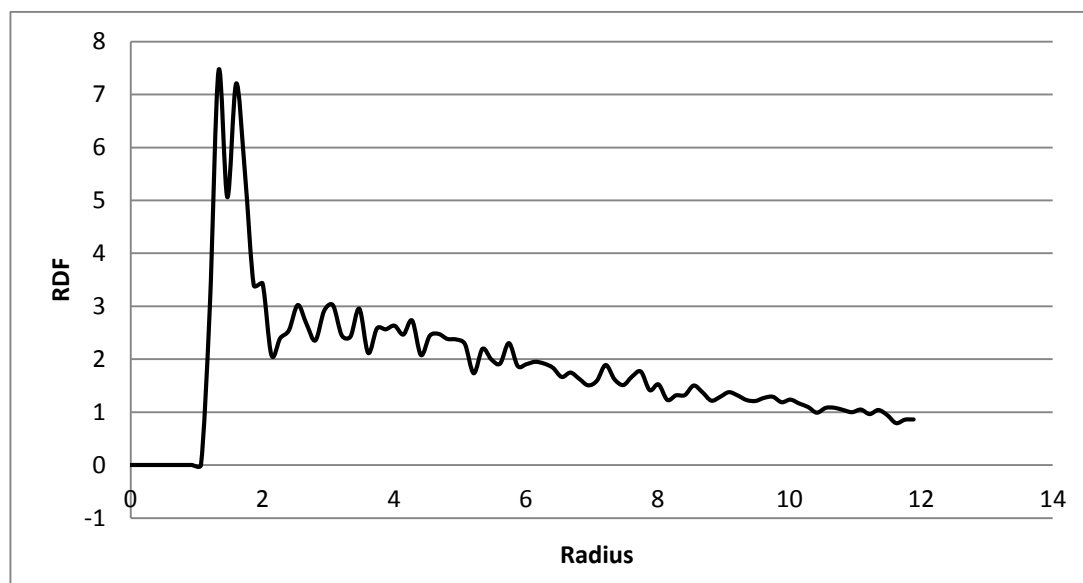
4D) Beads 20
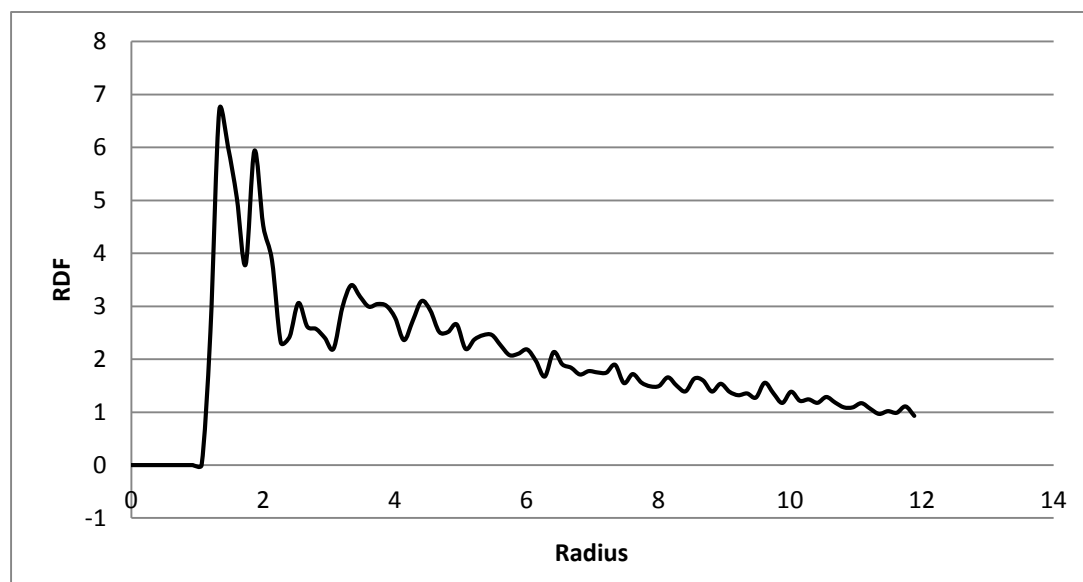
Figure 5)

5A) Peak at 5.0σ, Density = 0.00237
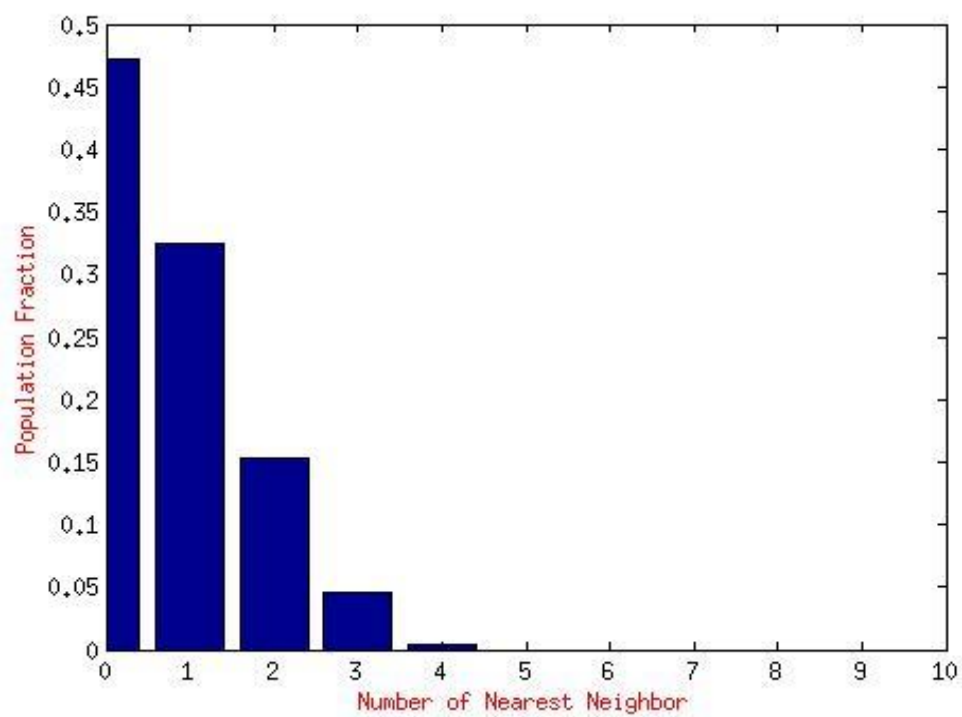
5B) Peak at 6.5σ, Density = 0.00237
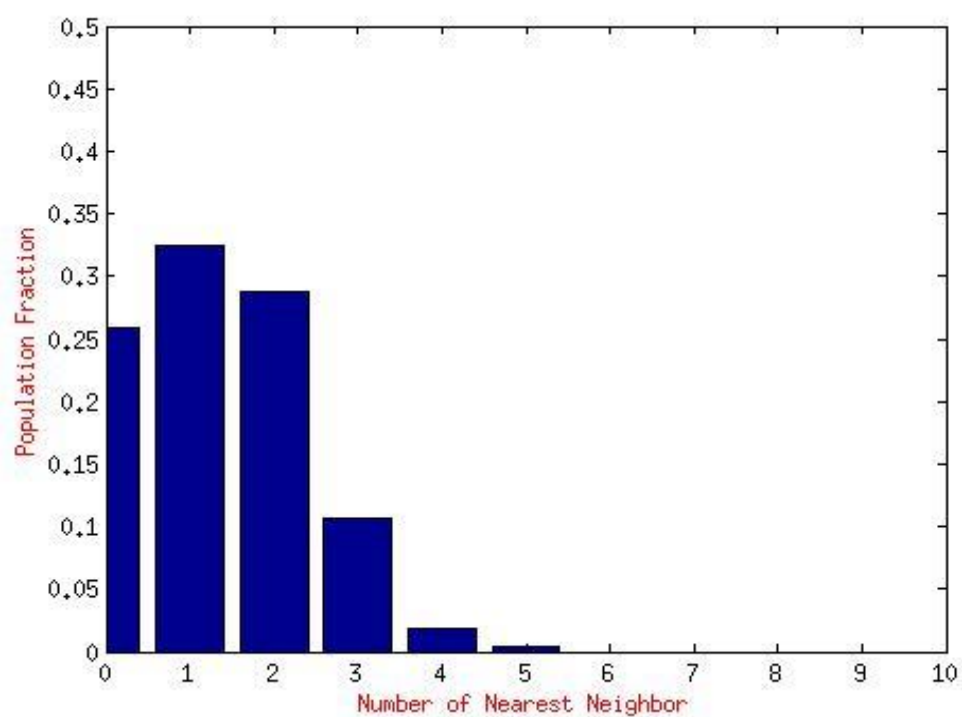
5C) Peak at 5.0σ, Density = 0.00078
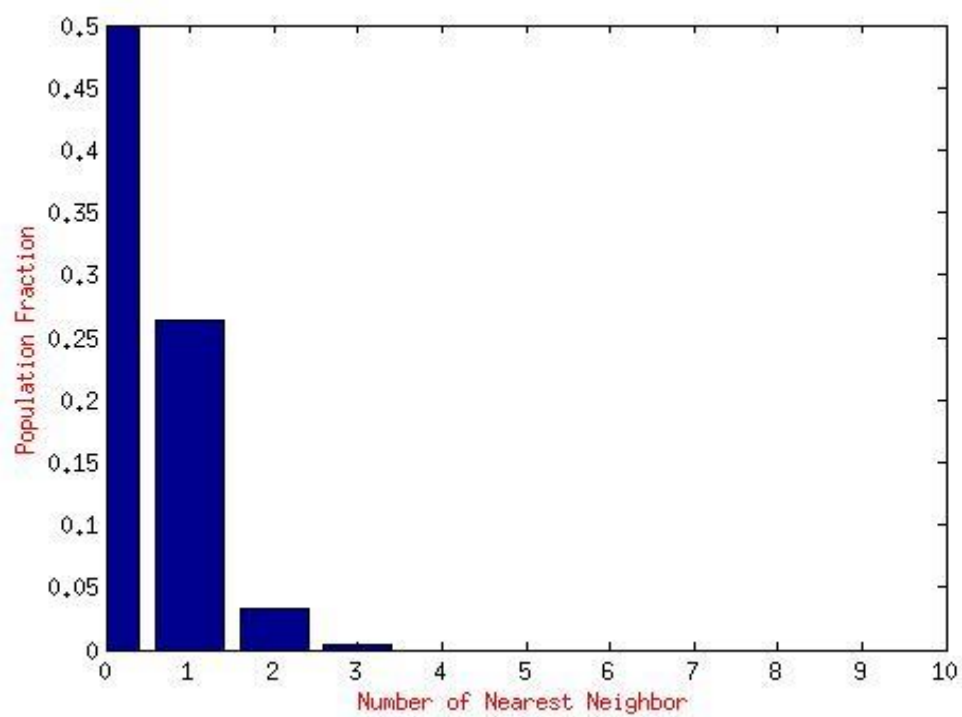
5D) Peak at 6.0σ, Density = 0.00078
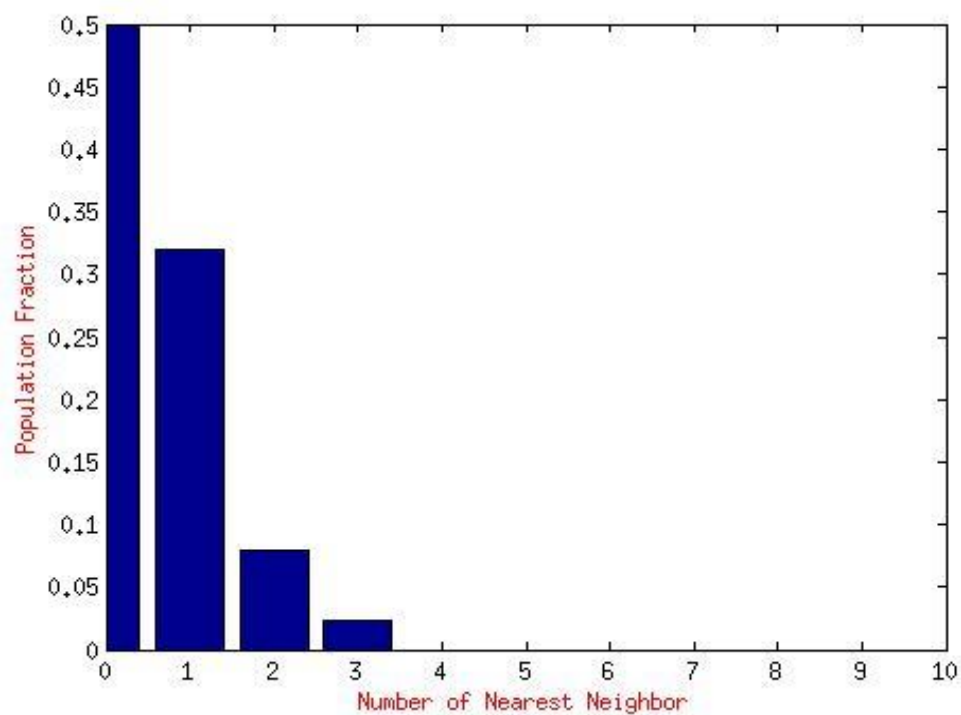
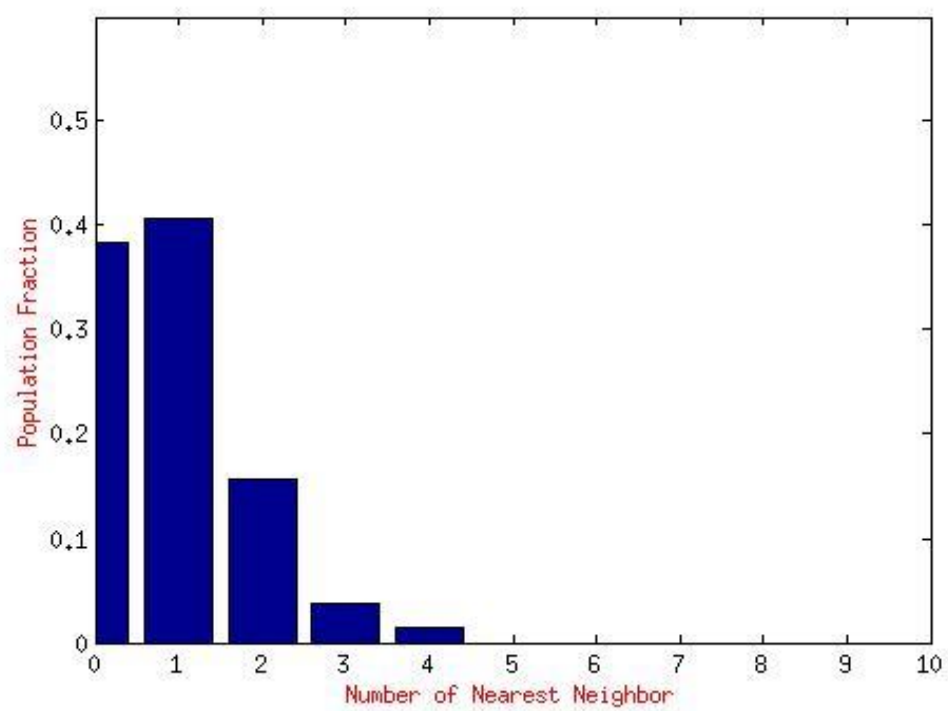**5E) Cumulative histograms for nearest neighbors at first or second nearest distances, Density = 0.00237**
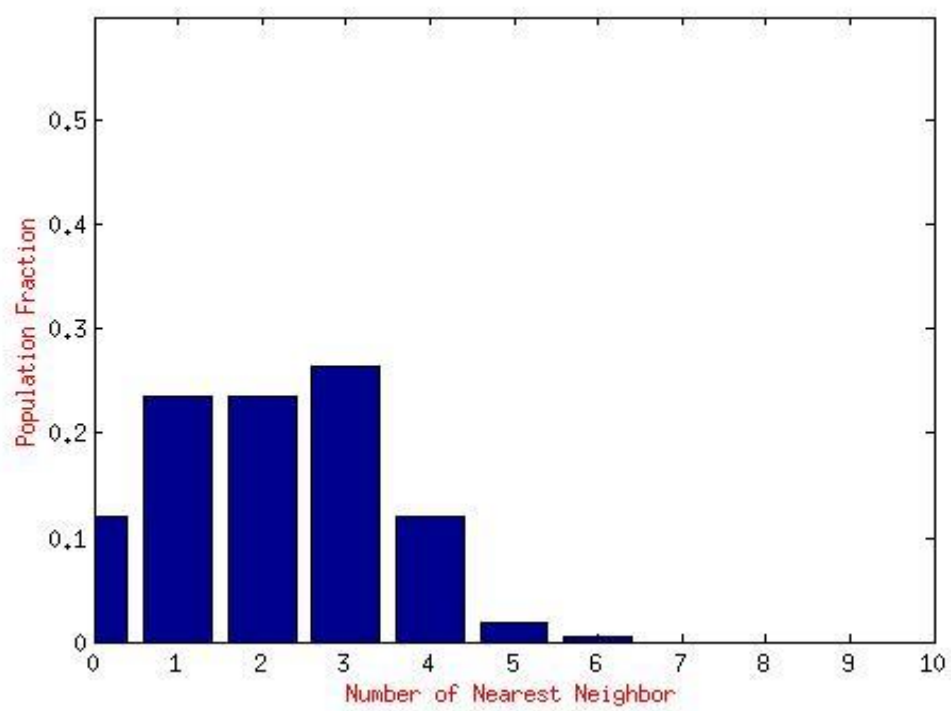
5F) Cumulative histogram for nearest neighbors at first or second nearest distances, Density = 0.00078

Figure 6

Cumulative Histograms for 1ˢᵗ and 2ⁿᵈ distances and Radial Distribution plots for anisotropies with 10 beads in tethers in a simulation box at high density of 0.001728 nanoparticles perσ³.

6A) Anisotropy (1D), peaks at 4.5σ and 6.0σ

6A-1)
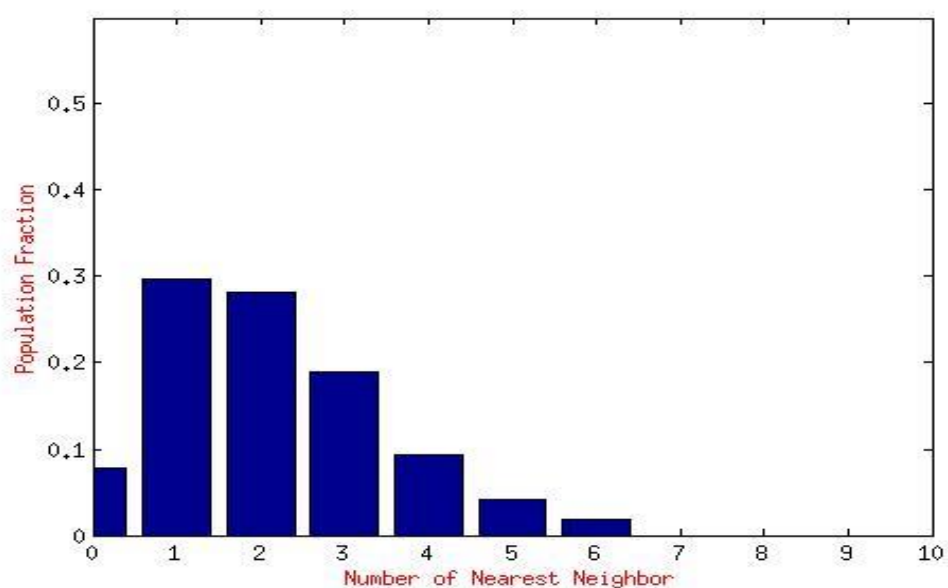
6A-2)
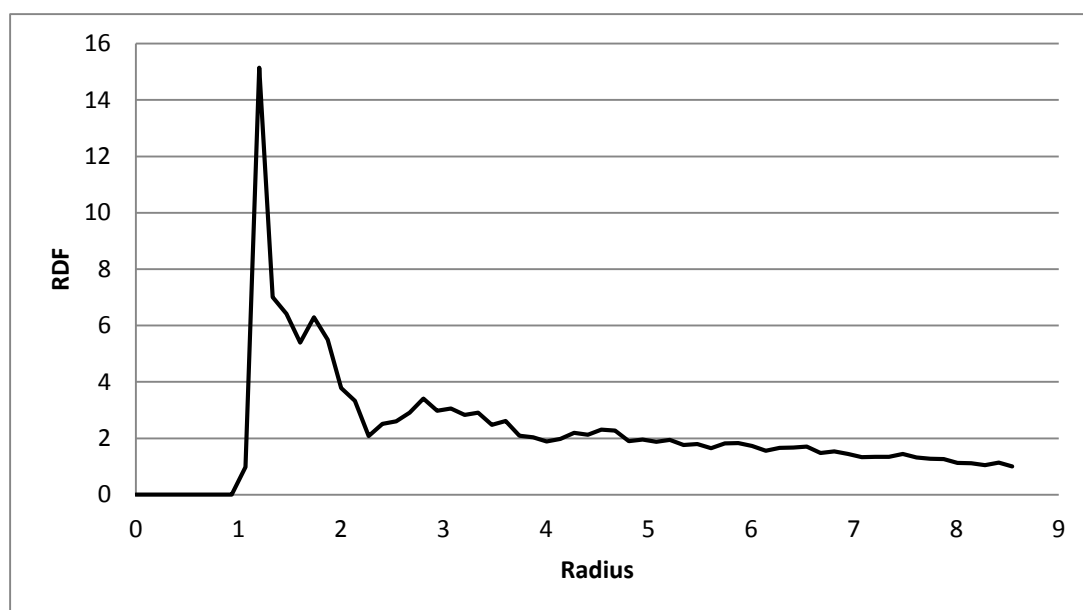
6B) Anisotropy (1E), peaks at 5.0σ and 6.5σ
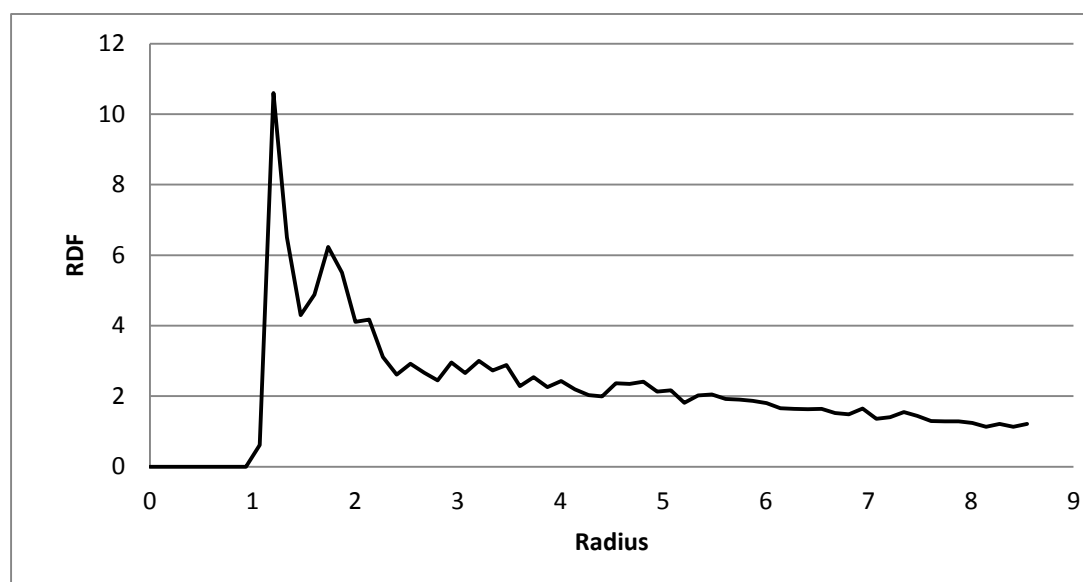
6B-1)
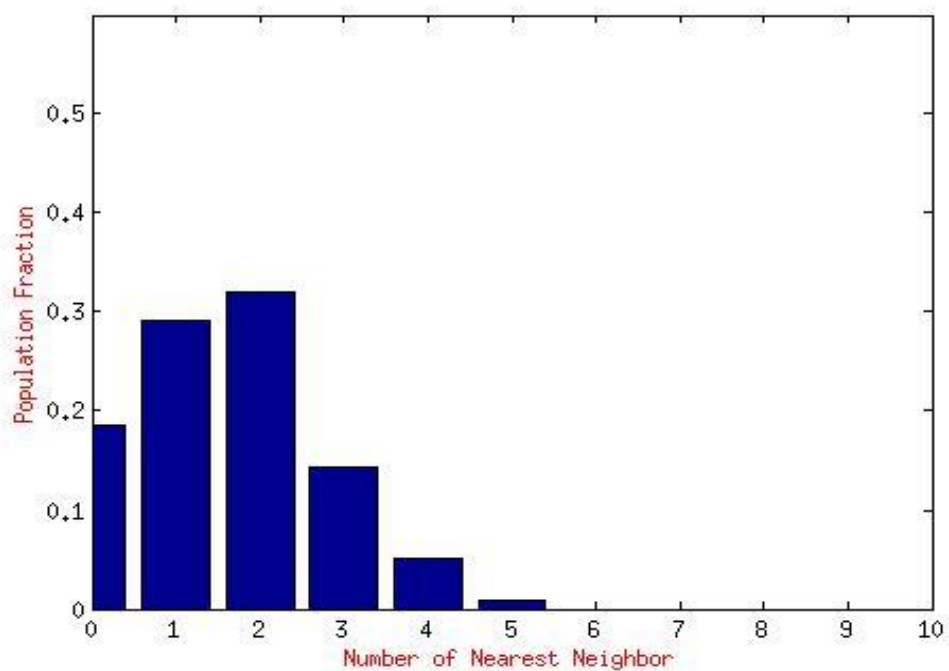
6B-2)
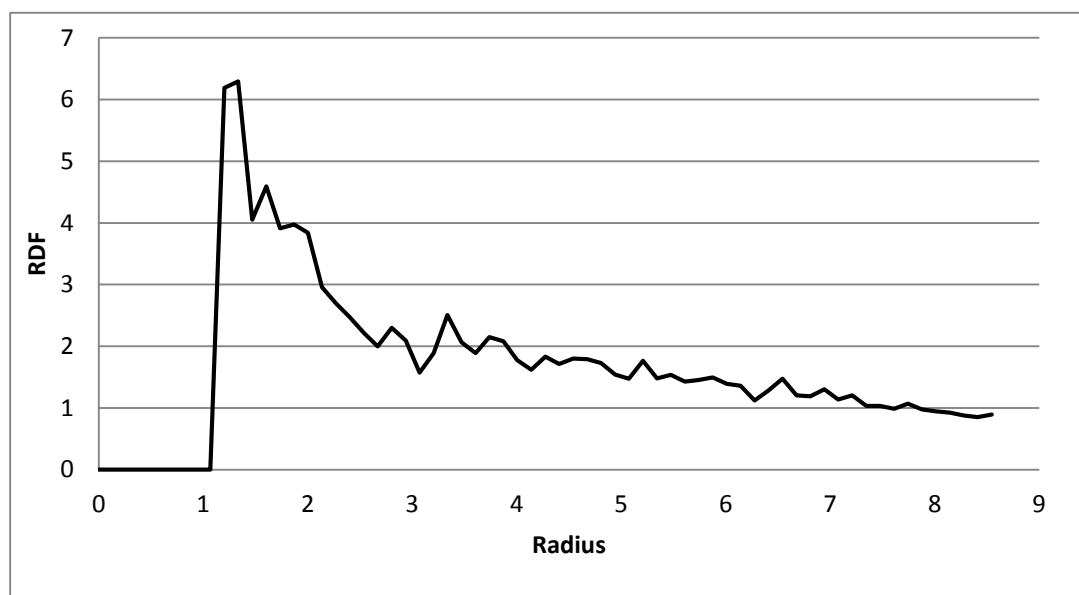
6C) Anisotropy (1F), peaks at 4.5σ and 5.5σ

6C-1)
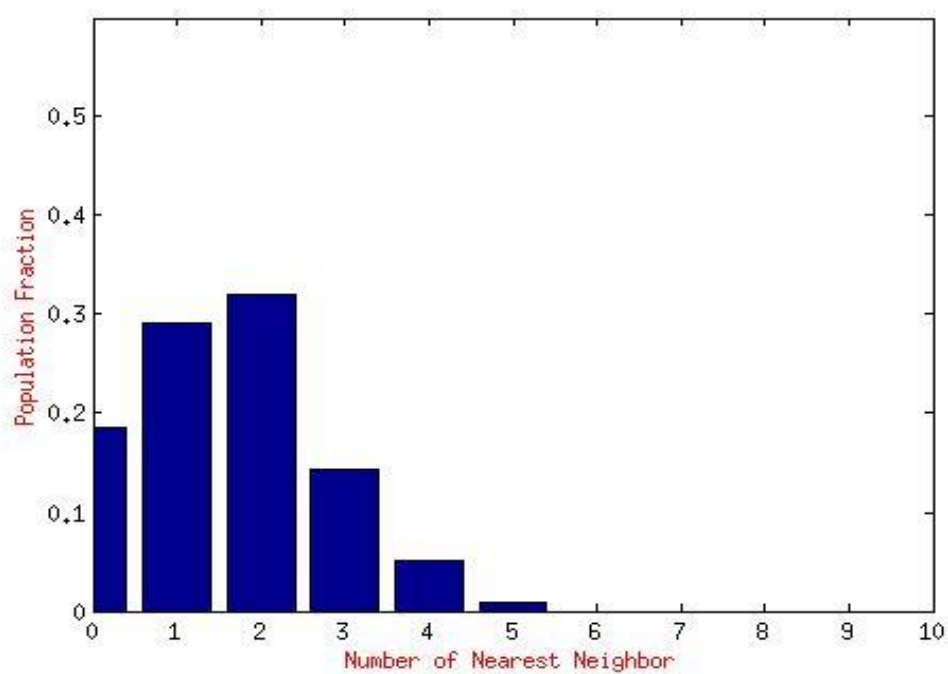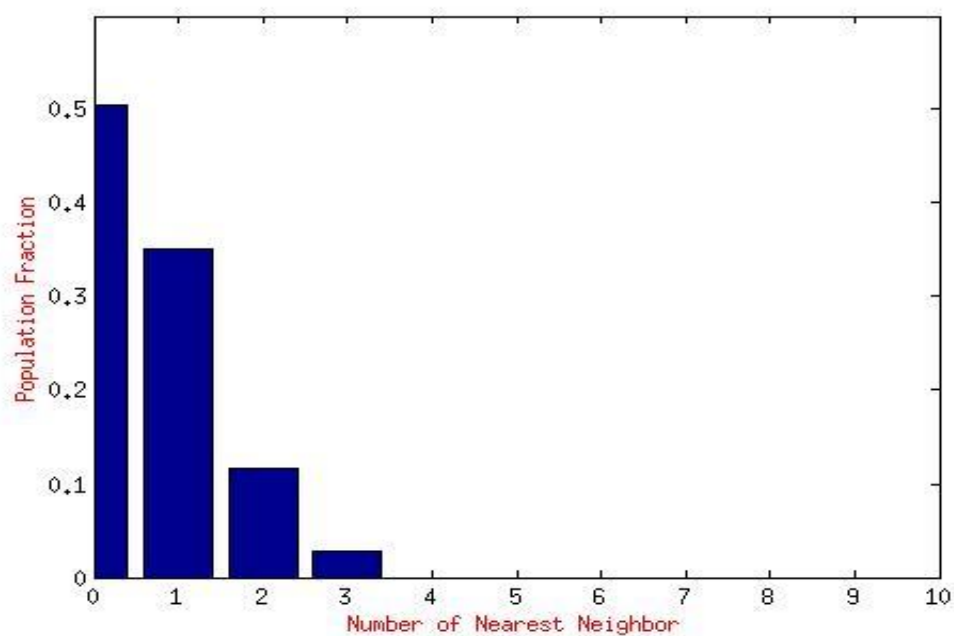

6C-2)
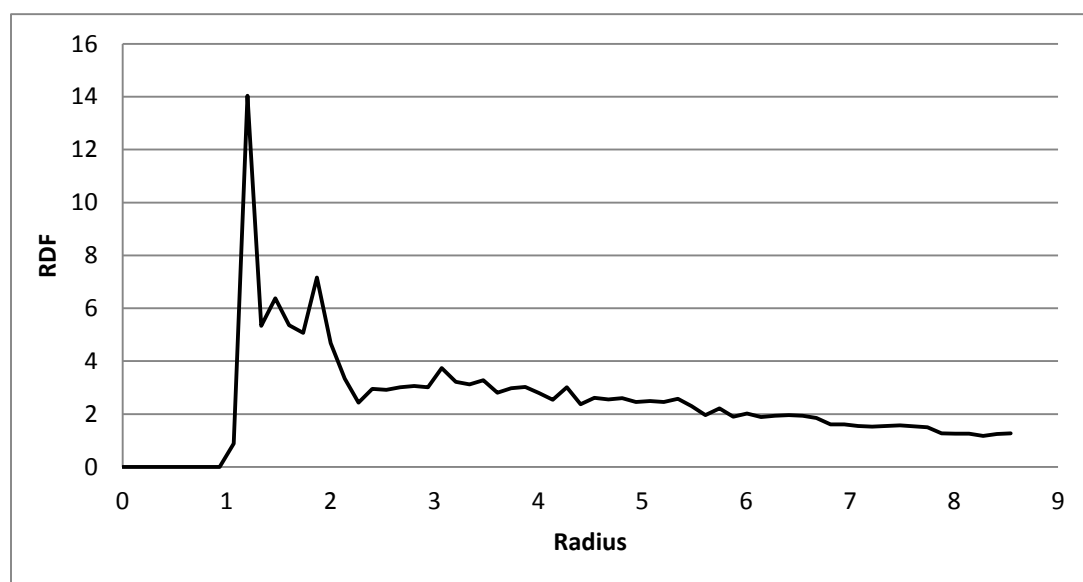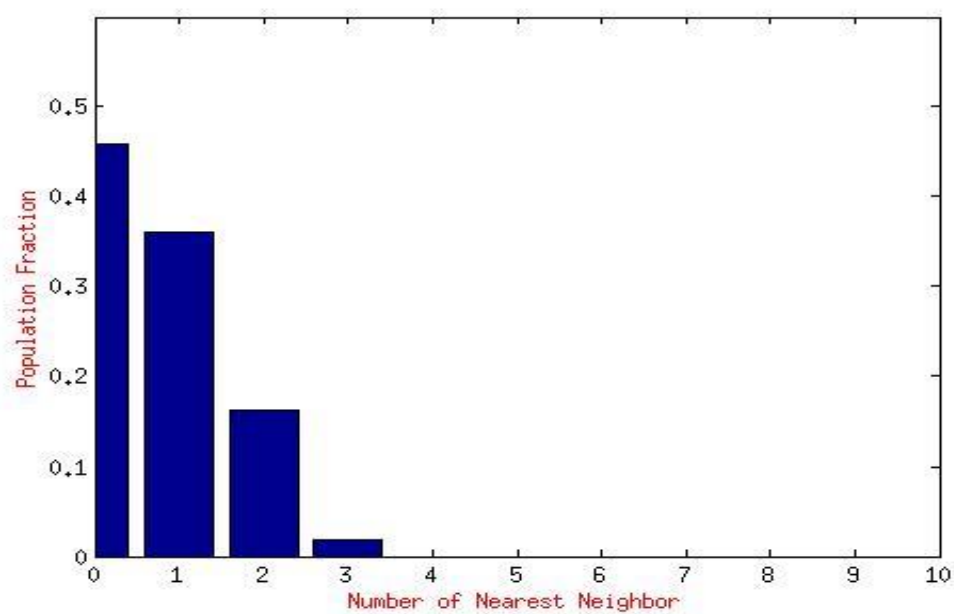
6D) Anisotropy (1G), peaks at 4.5σ and 7.0σ

6D-1)
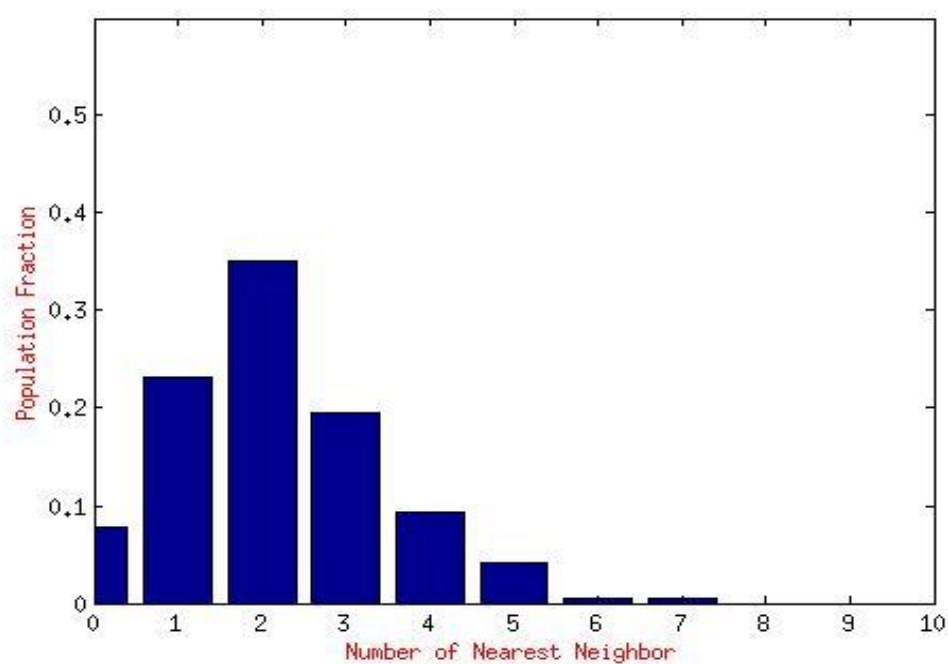
6D-2)

Cumulative Histograms for 1ˢᵗ and 2ⁿᵈ distances

E) Anisotropy (1F), Density= 0.000296

F) Anisotropy (1G), Density = 0.000296

Chapter 3.3

Chain type aggregates

As would be expected, chain type aggregates appear under both solvent conditions frequently. The radial distribution and histogram plots in Figure 7, show that the anisotropy in Figure 1B gives dimers and chains even for the low density system of 0.000296 nanoparticles per σ^3 (Figure 7F) while the high density systems are observed to aggregate into clusters (Figure 7C-E).

Also, the anisotropy 1C results in chain like arrangements which is captured in the radial distribution plots in Figure 9, and the corresponding fractional area (area under the peak/total area) for the individual peaks, showing several 2nd, 3rd and 4th neighbors for the high density systems. It can also be seen that for system with 5 beads in tethers, there is only one first neighbor distance at 4.5σ, while for other systems there is a second farther directly coordinating first neighbor at 6σ-7.5σ. We can say that these distances correspond to the directly coordinating atom because the second neighbors are expected at distances greater than 4.5X2σ.

Radial distribution plots for high density systems, under solvent conditions favoring the aggregation of nanoparticles is shown in figure 10. We observed a decrease in the first neighbor distance from 4.5σ to 4.0σ for all systems except 1A. This is attributed to the direct placement of the nanoparticles with each other as against aggregation through tethers. The aberration from this norm for 1A can be due to the formation of larger clusters

owing to the lower excluded volume of this compared to the other systems under the given solvent conditions, which would also facilitate formation of N-mer type

aggregates as also confirmed from the histogram in 10A. The slight increase in the fraction of uncoordinated atoms can also be noticed in 10C-G. While we observe some strong bands in coordination number 3 of the histogram plots for 10E, other systems (10 C, D, F, G) show several dimers and chain like arrangements (corresponding to band in coordination numbers 1 and 2 respectively) as in Figure 11 I- J. Also, it can be noted that even the 6 tethered nanoparticle can arrange in chains and even in sheets as in Figure 11 H. At lower densities we observed an overall decrease in coordination numbers but no change in the emerging structures.
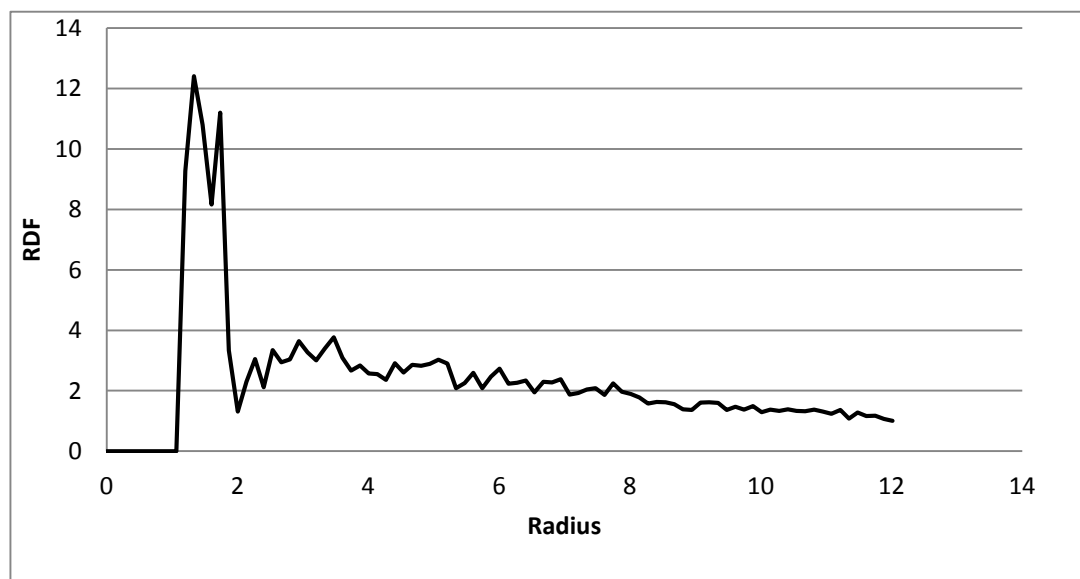
Figure 7)

Chain like aggregates, Anisotropy in 1B, Number of beads in tether =10, solvent conditions such that tethers aggregate: RDF and cumulative histograms
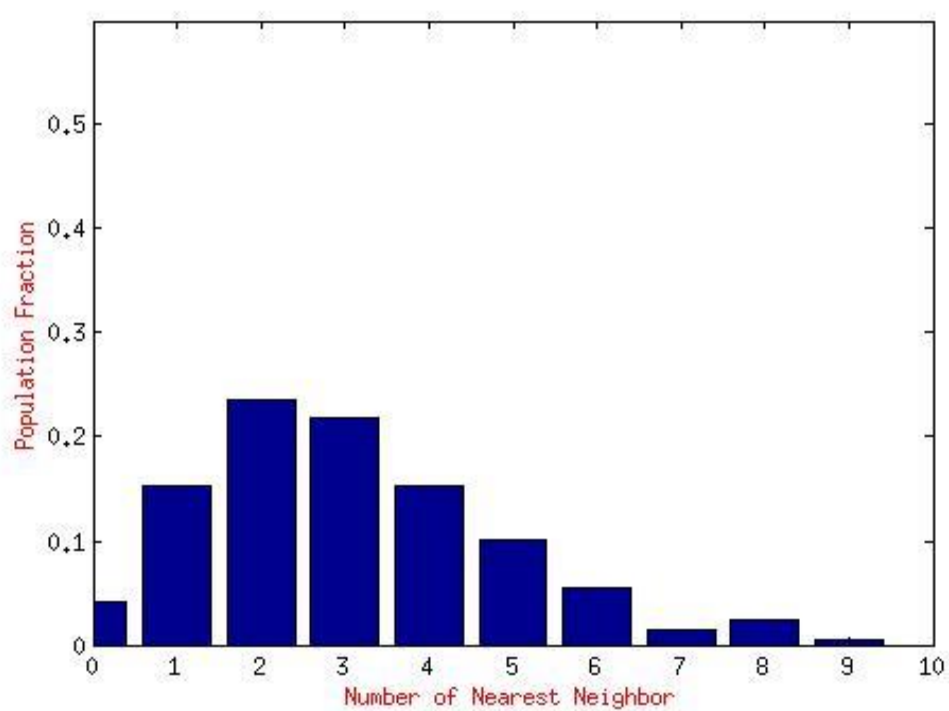
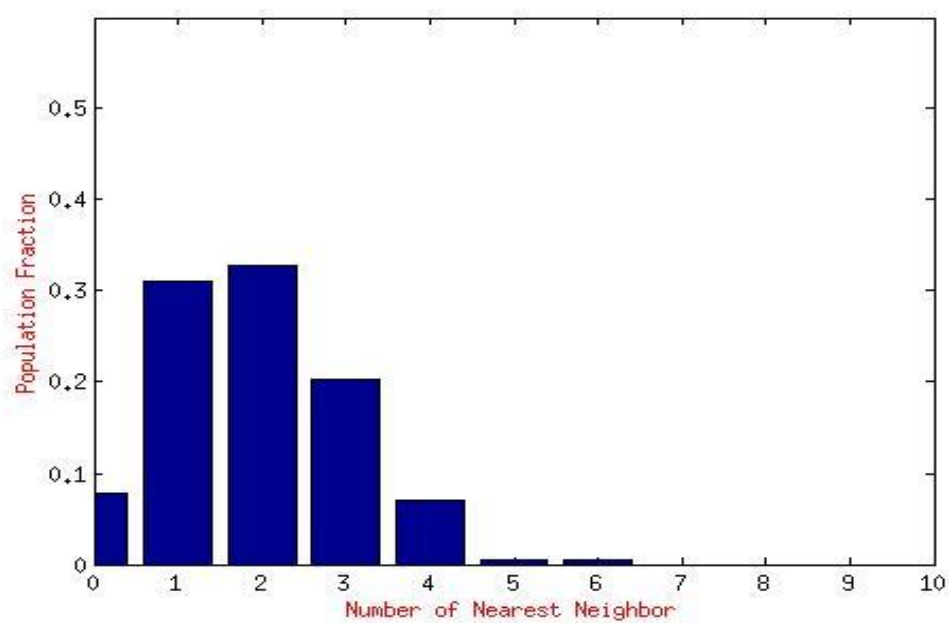**7A)Radial Distribution at a density of 0.00237, Peaks at 5.0σ and 6.5σ**
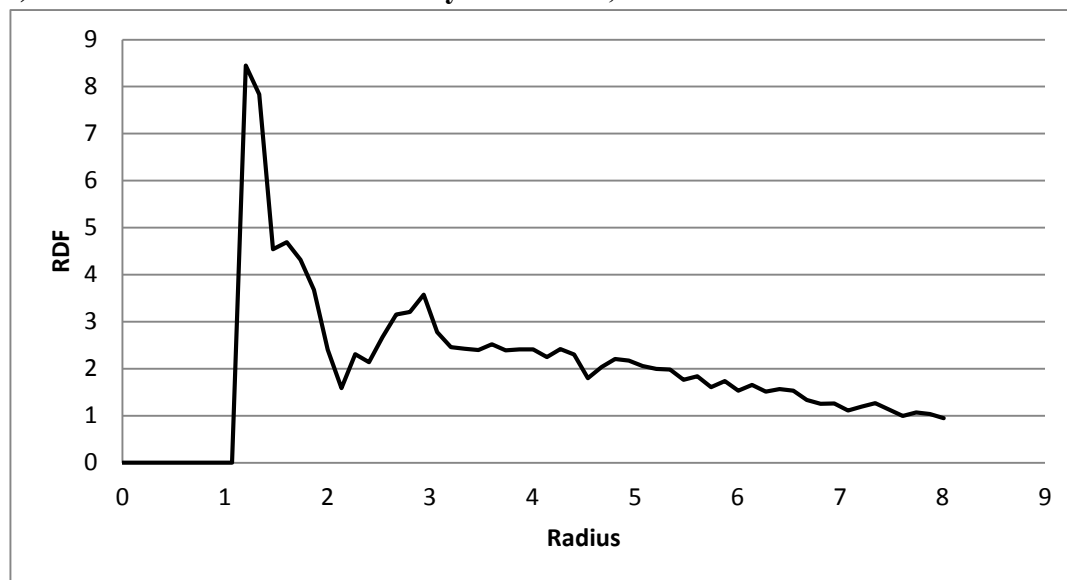
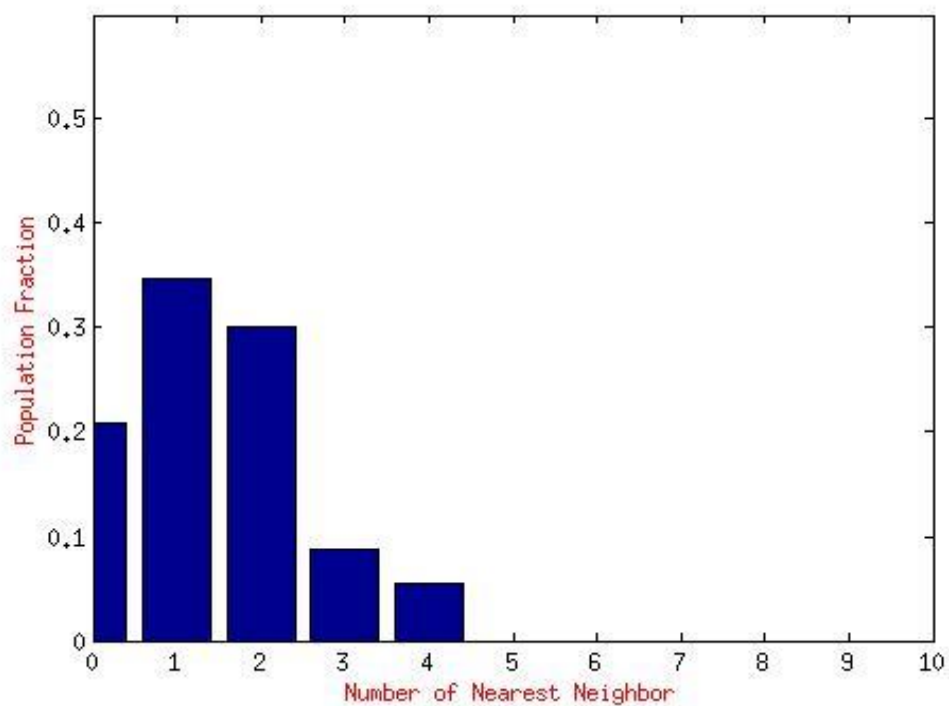**7B) Radial Distribution at a density of 0.00078, Peaks at 5.0σ and 6.5σ**

7C) Density = 0.00237

7D) Density = 0.001298

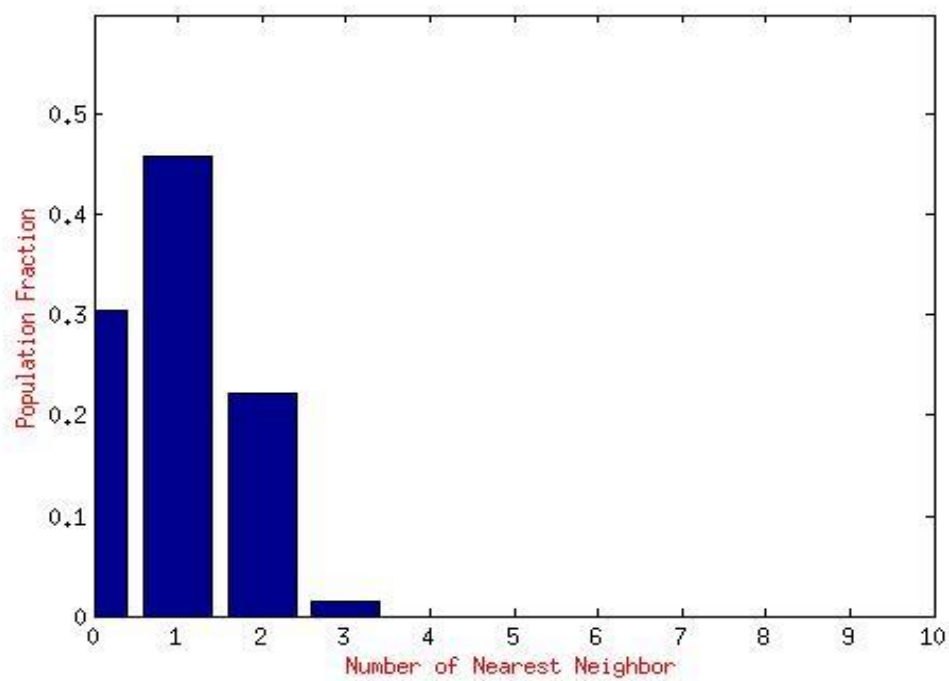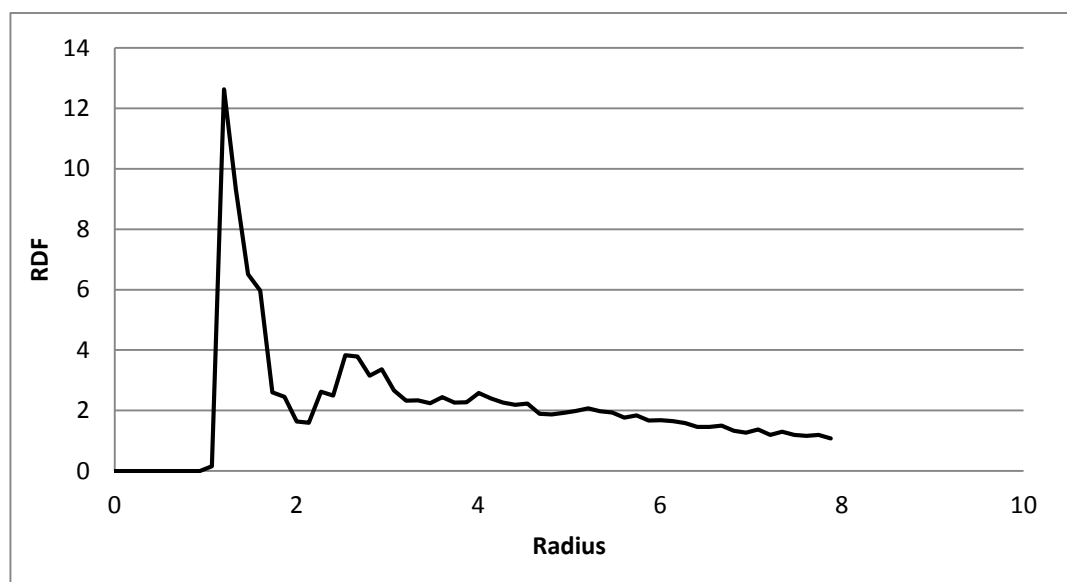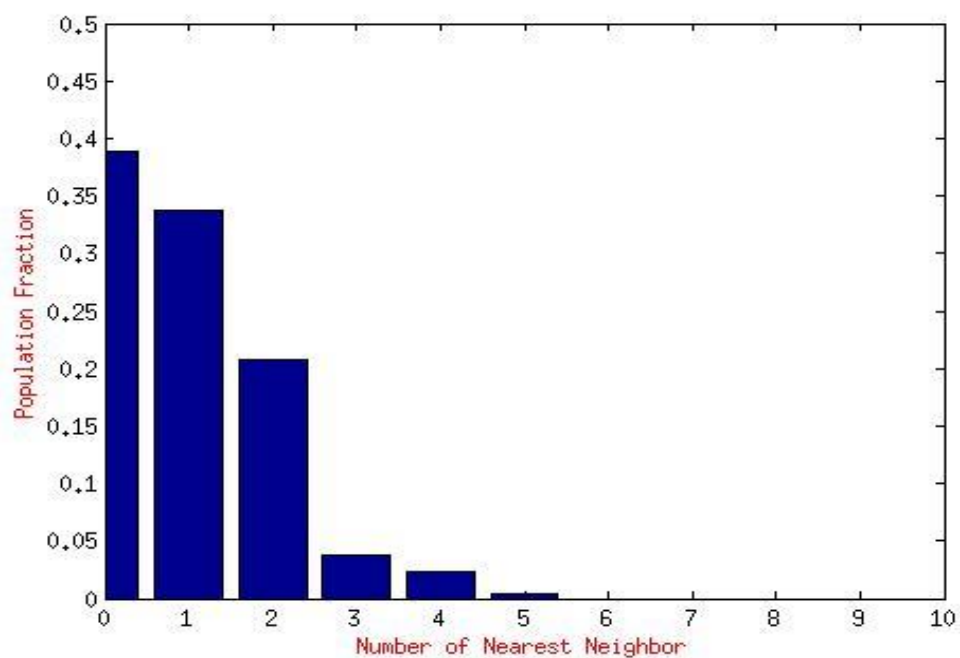**7E) Density = 0.000787**

7F) Density = 0.000296

Figure 8)

Anisotropy in (1C) under conditions favoring the attraction of tethers, Number of beads in tethers= 5
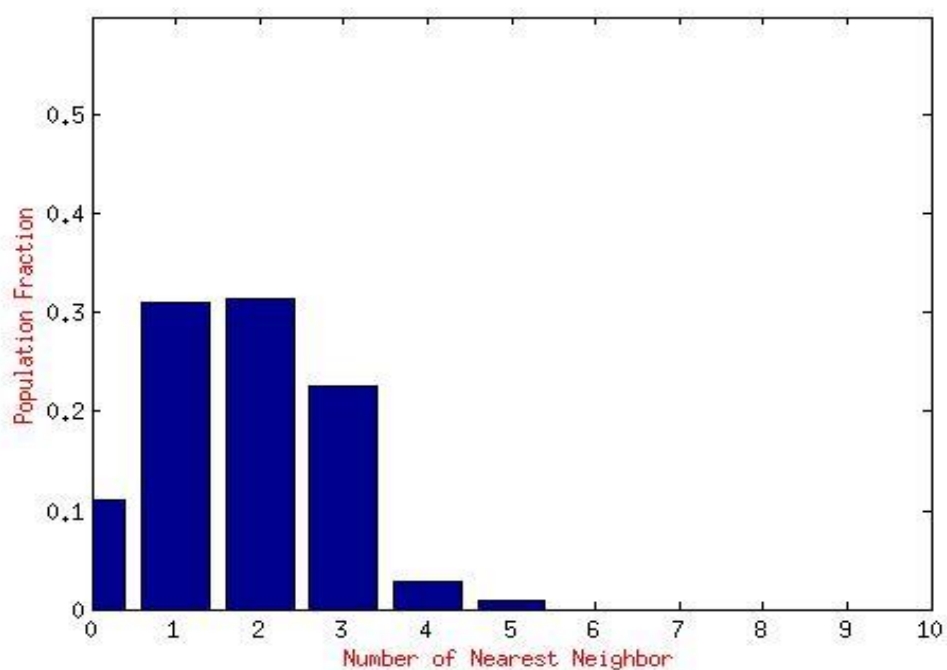
8A)Radial Distribution at density = 0.00237

8B) Histogram for peak at 4.5 at Density = 0.00237

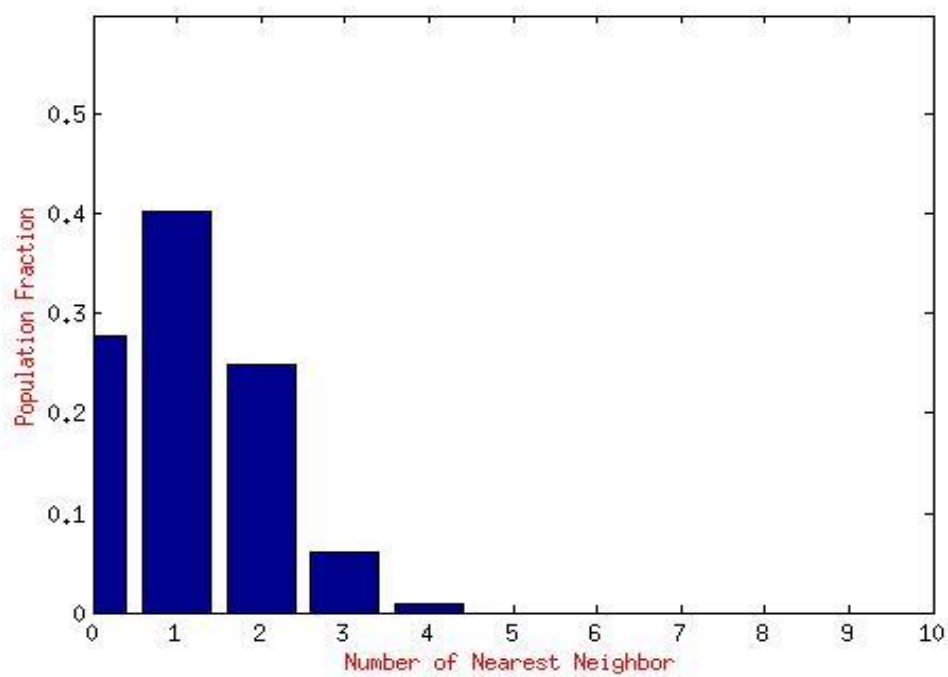**8C) Cumulative Histogram for peaks at 5.0 and 6.0 for Density = 0.000787**

8D) Cumulative Histogram for peaks at 4.5 and 6.0 for Density = 0.000296

Figure 9

Radial Distribution Plots for simulations run under conditions favoring the aggregation of tethers in anisotropy 1C for different tether lengths with a high density of 0.00237 and tabulated is fractional area under the peaks at different distances (σ units)
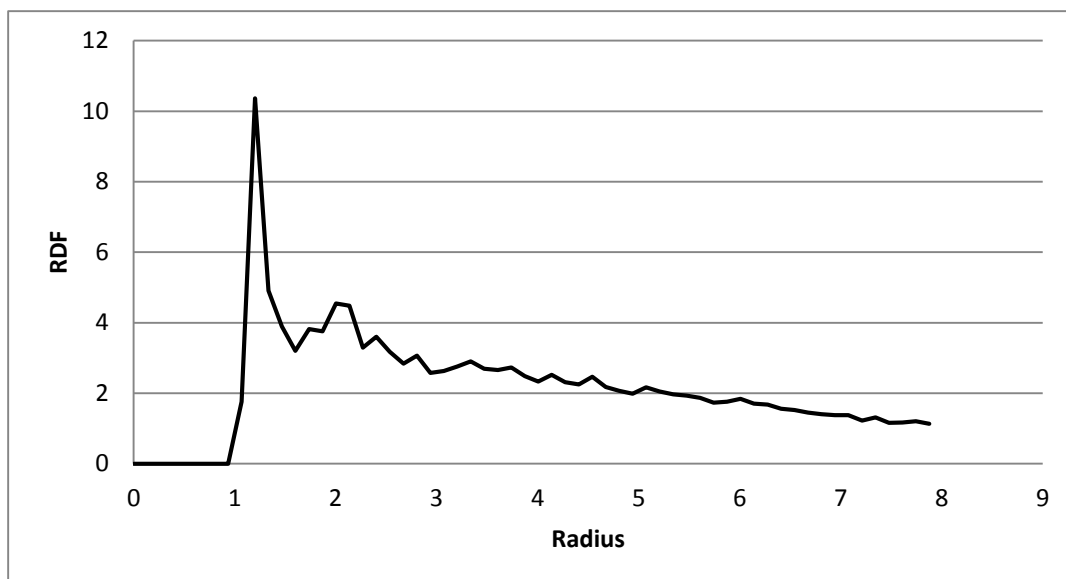
9A) 5 beads ,
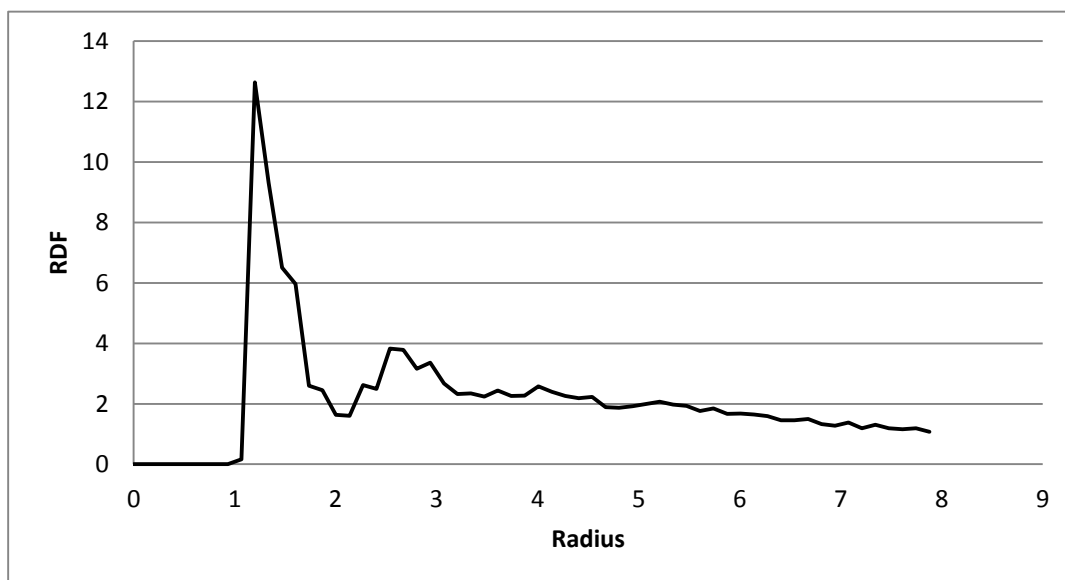
Distance (σ)	Area under the peak
4.5	**0.262411**
10	**0.187775**
13	0.0448427
15	**0.0640664**
16.5	0.0283475
17.5	0.0269157
19.5	**0.0788938**
22	0.0462659
23.5	0.0301919
25	0.0456584

9B) 10 beads
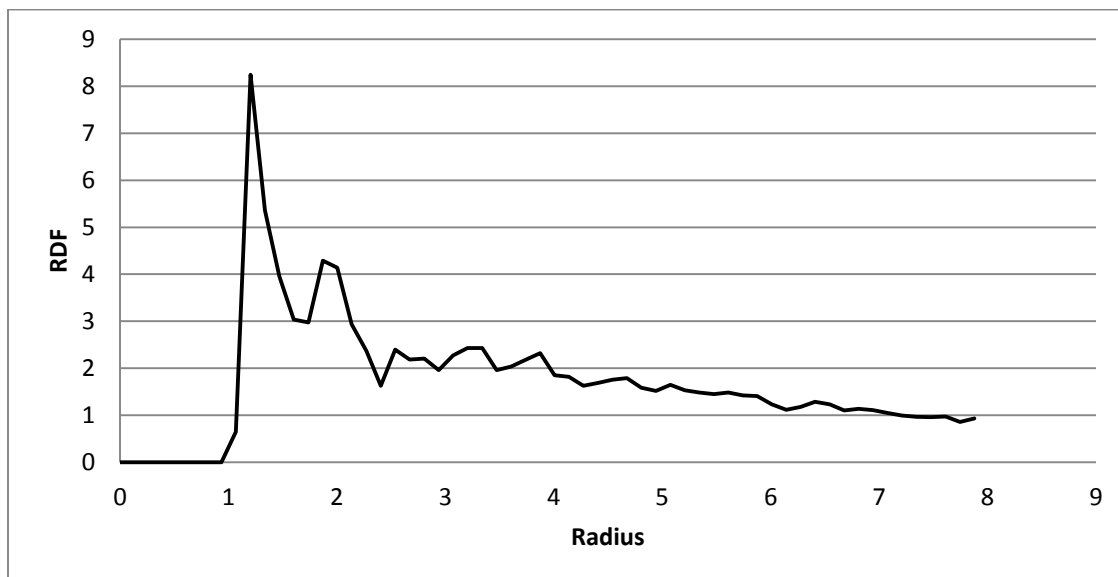
Distance (σ)	Area under the peak
4.5	**0.164974**
7.5	**0.168338**
12	**0.128892**
14.5	**0.113088**
17.5	0.042607
18.5	0.0268371
19.5	0.037712
21.5	**0.0560911**
24	**0.0507765**
26	0.0265983

9C) 15 beads

Distance (σ)	Area under the peak
4.5	**0.150835**
7	**0.127685**
9	**0.0424157**
10	**0.0572458**
11.5	0.0376835
12.5	**0.0533526**
14.5	**0.0508369**
15.5	0.0319117
17	0.06026
18.5	0.0277023

9D) 20 beads,
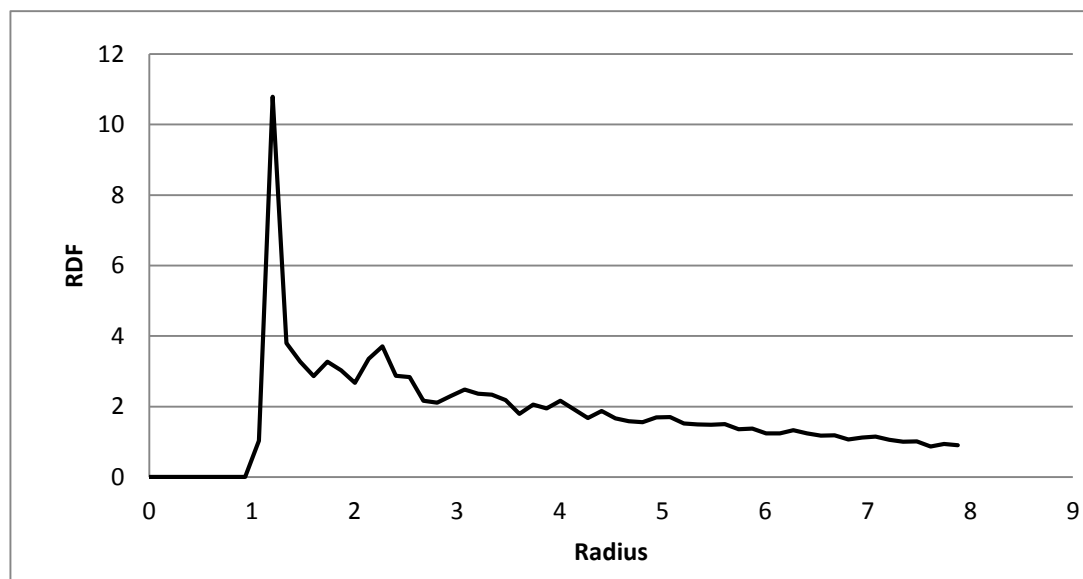
| Distance (σ)	Area under the peak
4.5	**0.145552**
6	**0.0939389**
8.5	**0.136041**
11.5	**0.0584985**
12.5	**0.0670211**
14.5	**0.0510061**
16	0.0430204
17.5	0.0270793
18.5	0.0520372
20.5	0.0358272

Figure 10)

Solvent conditions favoring the aggregation of nanoparticles, Beads 10, Density = 0.00237, Radial Distribution and Histogram Plots.

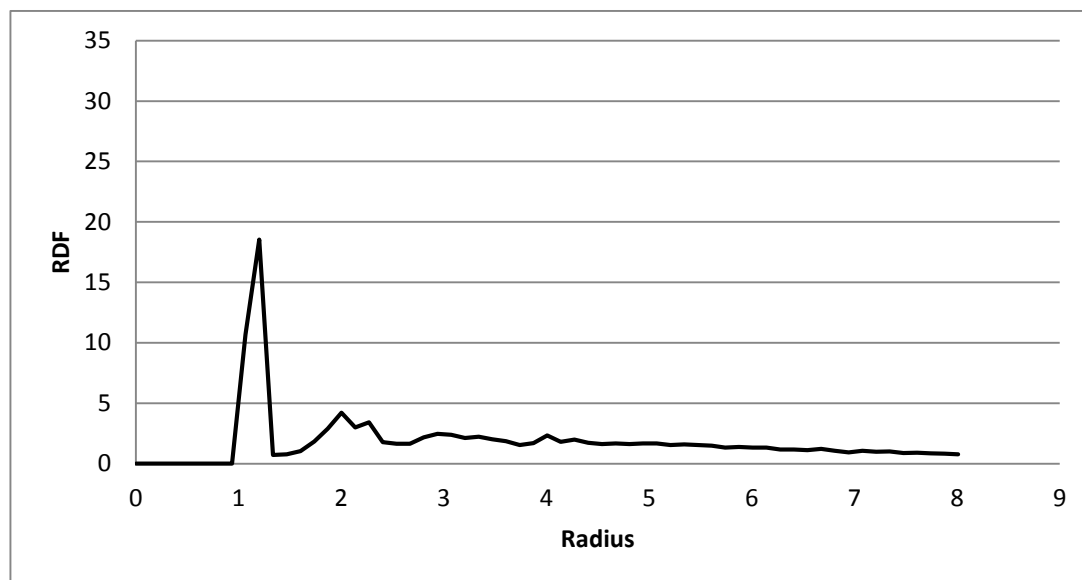**10 A) Anisotropy 1A, nearest neighbor peak at 4.5σ and corresponding histogram.**
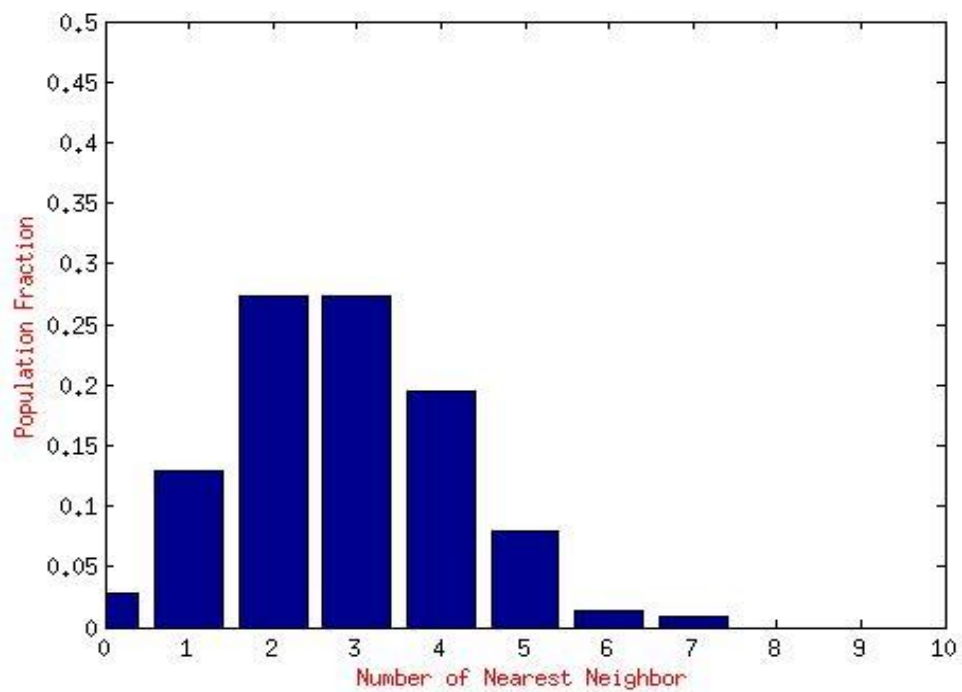
10A-1)
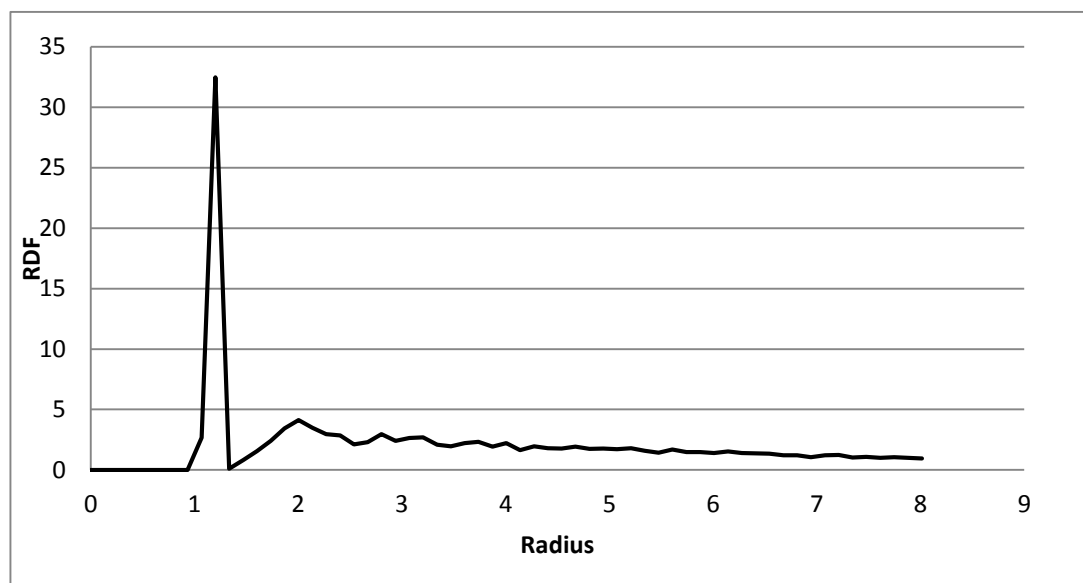
10A-2)
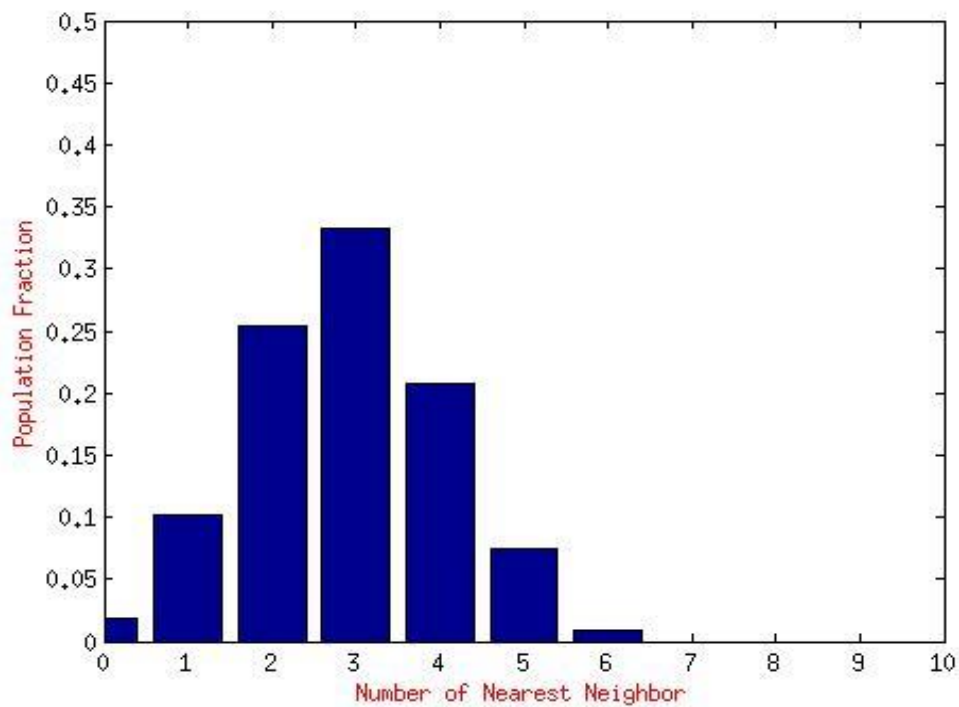
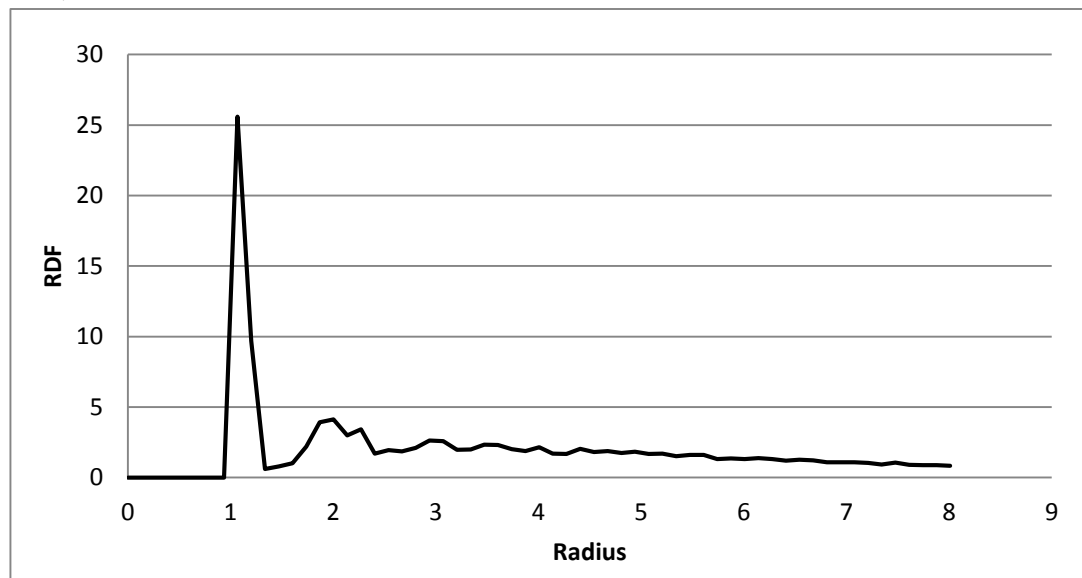**10B) Anisotropy 1B, nearest neighbor peak at 4.0σ and corresponding histogram.**
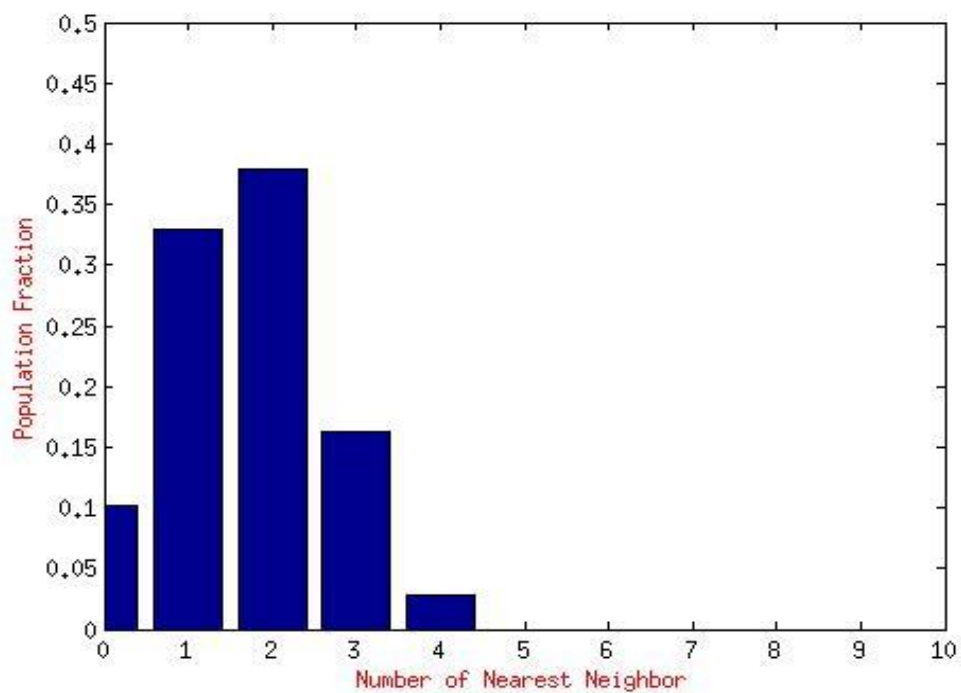
10B-1)

10B-2)

10C) Anisotropy 1C, nearest neighbor peak at 4.0σ and corresponding histogram.

10C-1)

10C-2)

10D) Anisotropy 1D, nearest neighbor peak at 4.0σ and corresponding histogram.

10D-1)

10D-2)

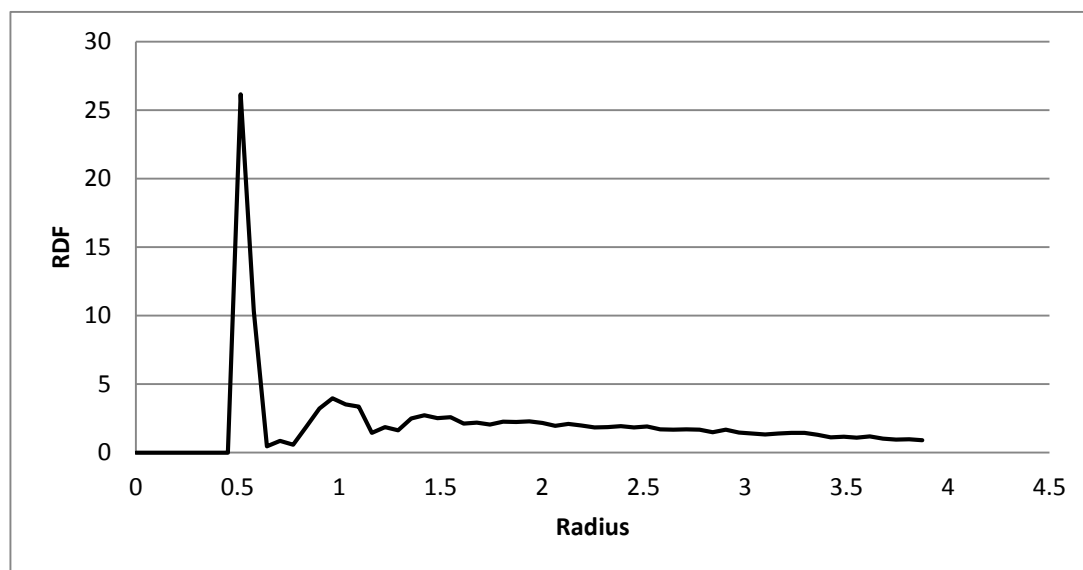**10E) Anisotropy 1E, nearest neighbor peak at 4.0σ and corresponding histogram.**

10E-1)
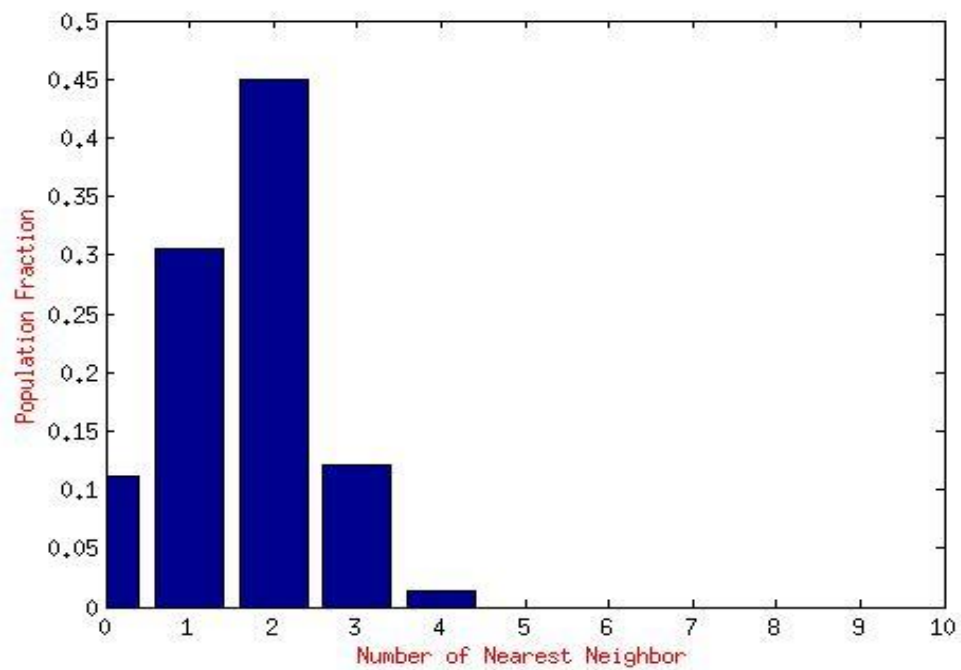

.

10E-2)

10F) Anisotropy 1F, nearest neighbor peak at 4.0σ and corresponding histogram.

10F-1)

10F-2)

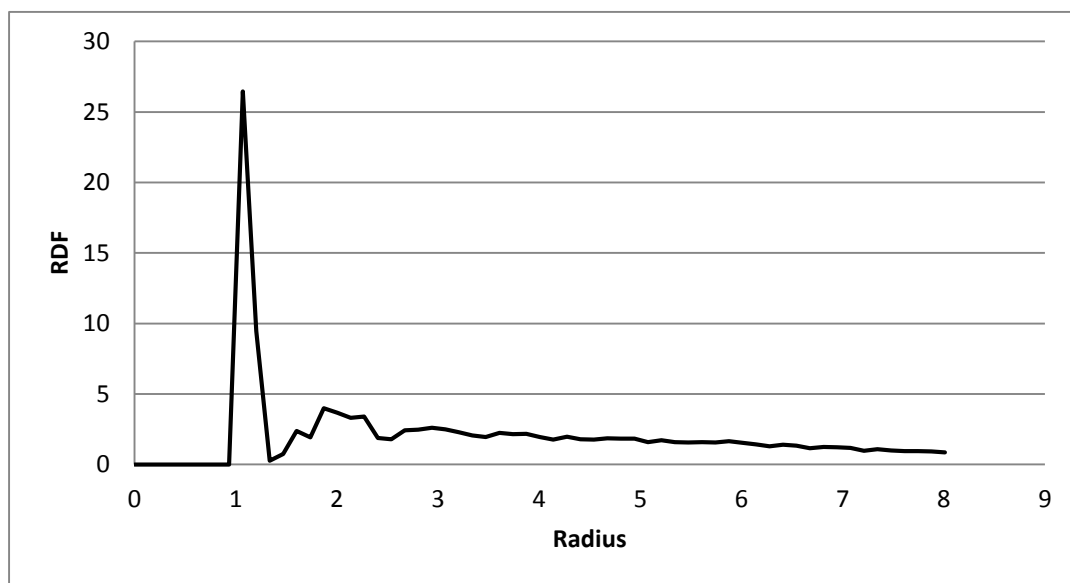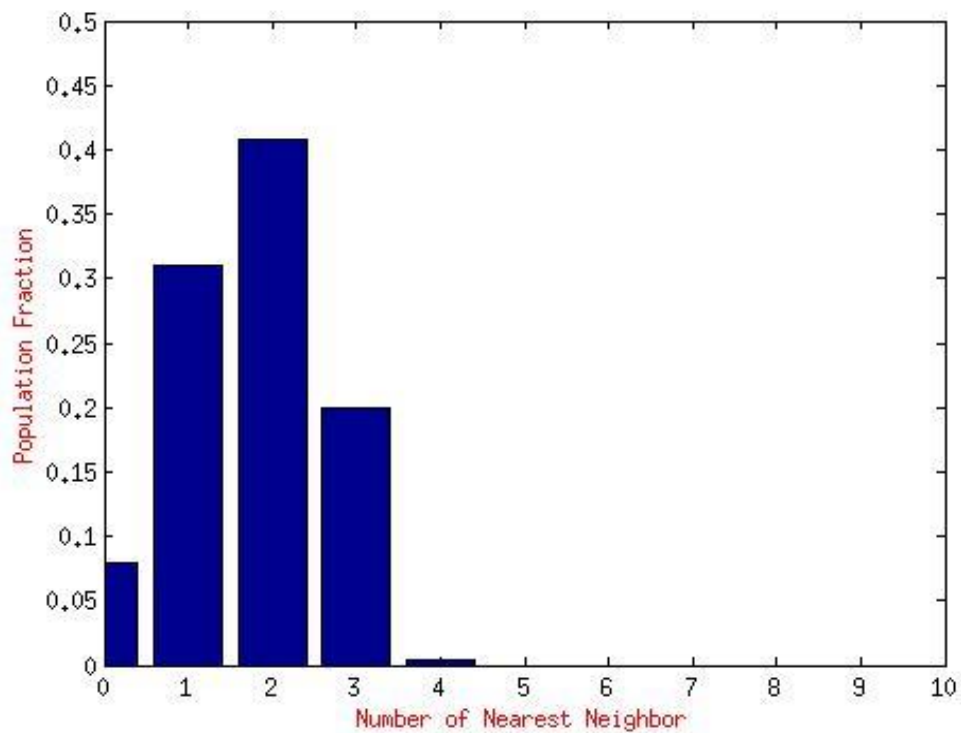**10G) Anisotropy 1G, nearest neighbor peak at 4.0σ and corresponding histogram.**
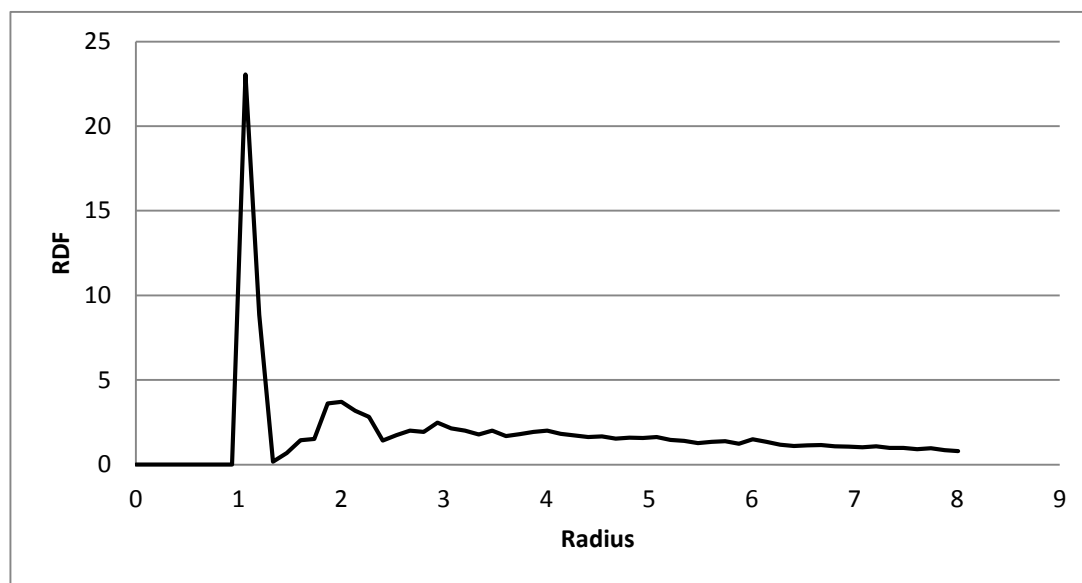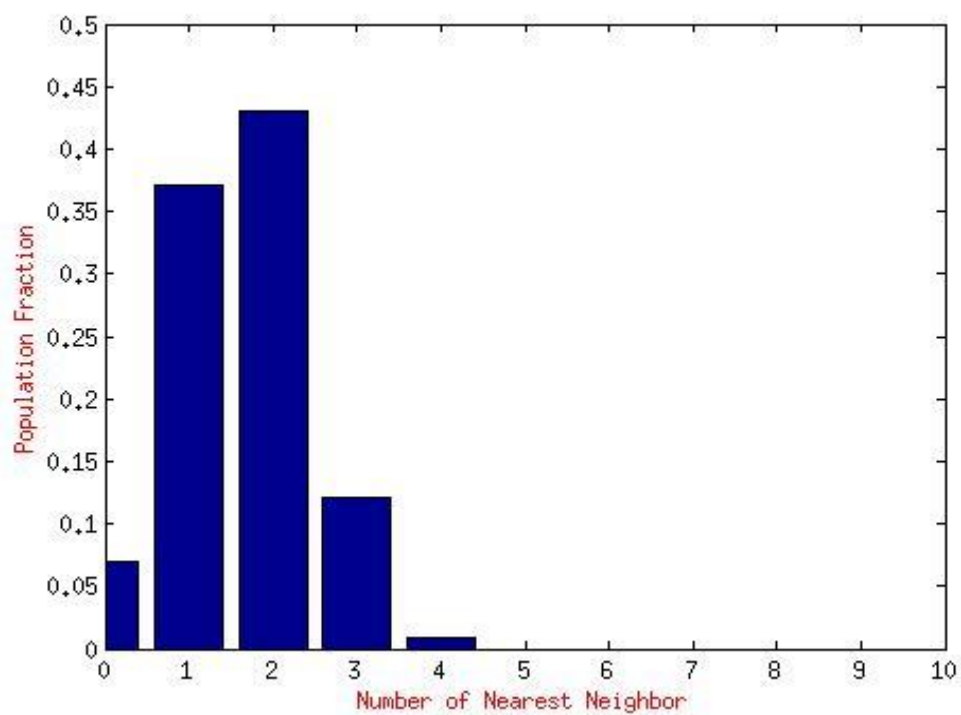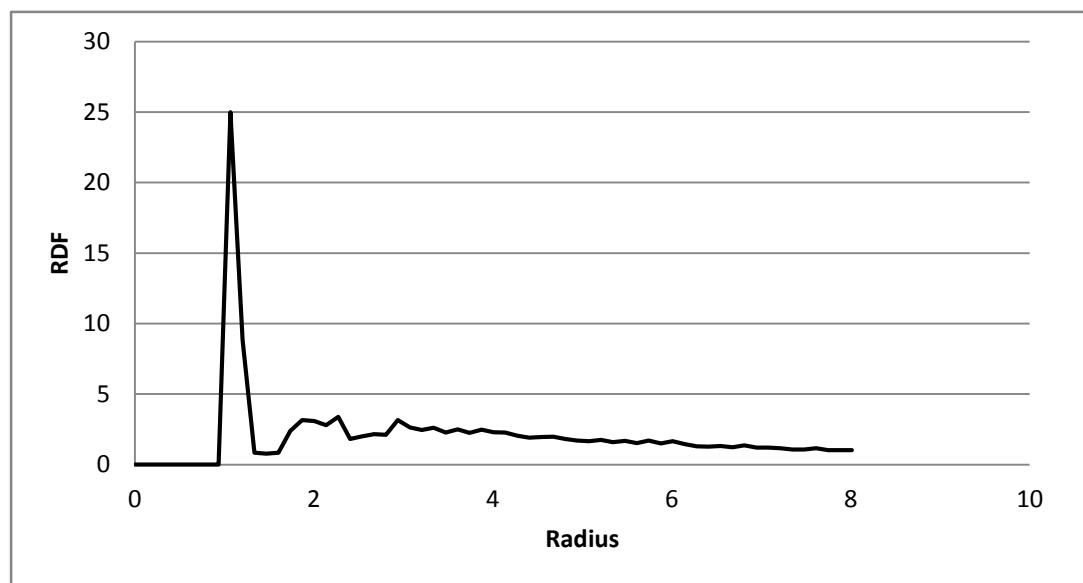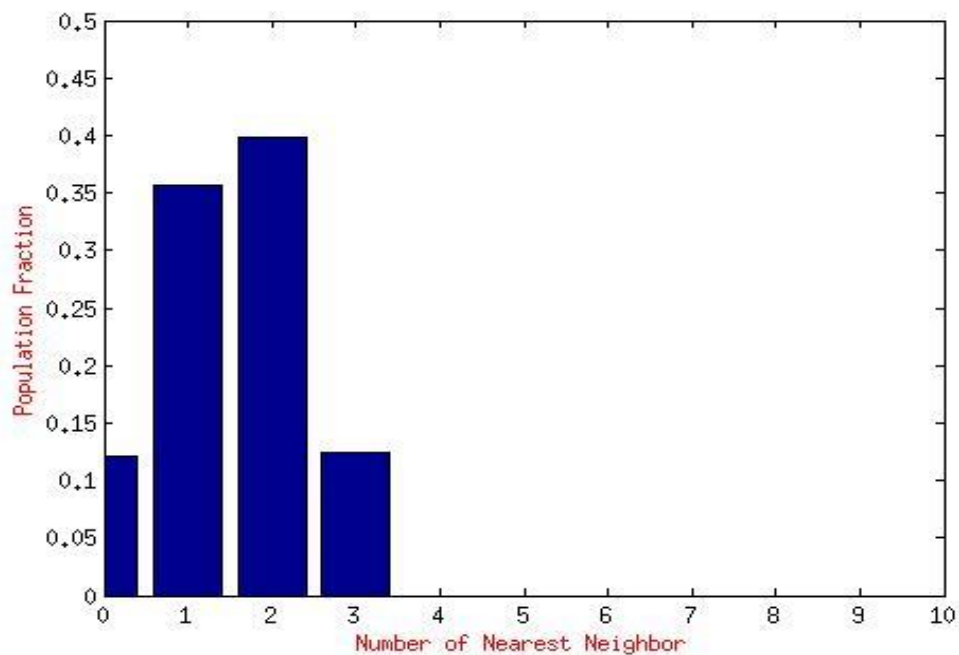
10G-1)

10G-2)

Chapter 3.4

2- Dimensional patterns and clusters

As shown in Figure 11 F and G, the anisotropies in 1D and 1G with 4 and 6 tethers respectively can potentially arrange themselves into sheets and 3D networks. These structures were observable in systems with 5 tether beads because under the solvent conditions favoring attraction in tethers, tethers of the same nanoparticle interact strongly with one another preventing interactions with other nanoparticle. This can be confirmed by the formation of several dimers even in systems with 5 tether beads for anisotropies 1C and 1E (Figure 2 G-H).

Figure 11)

11A) 2 Tethers as in 1B
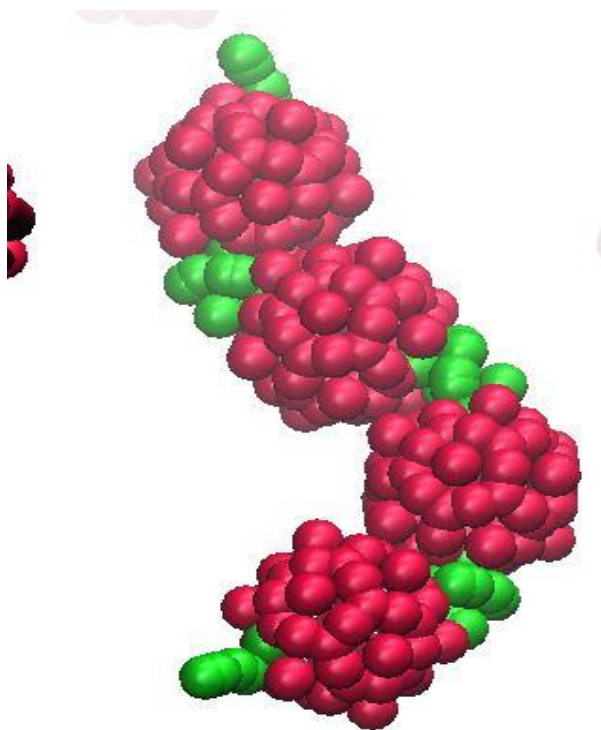
11B) 4 tethers as in 1C
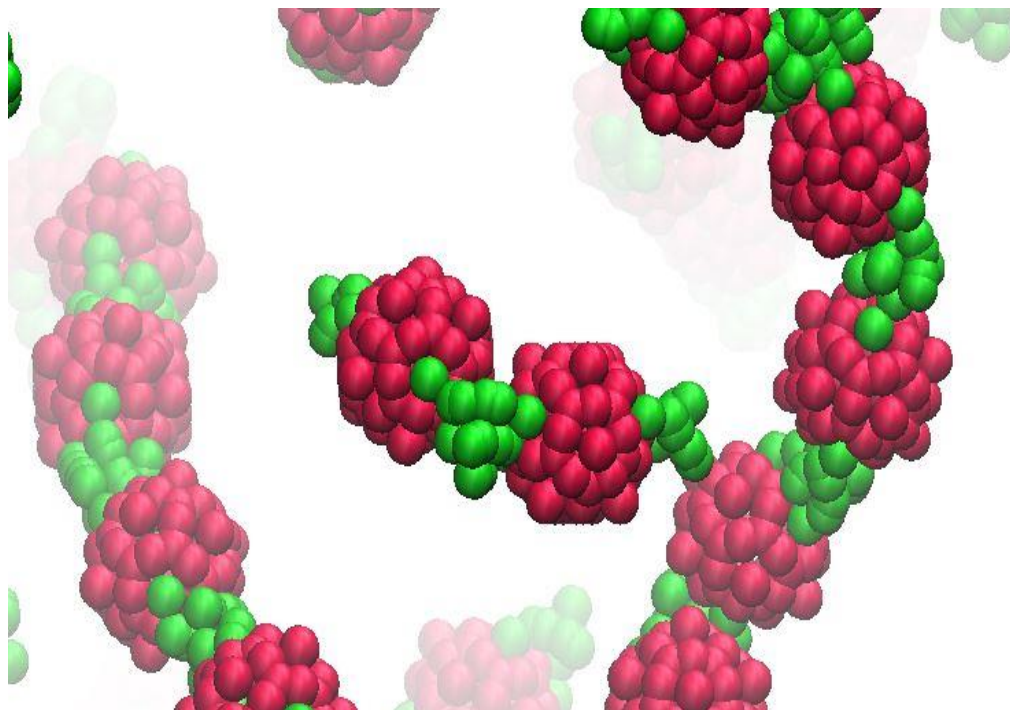
11C) 4 tethers as in 1D
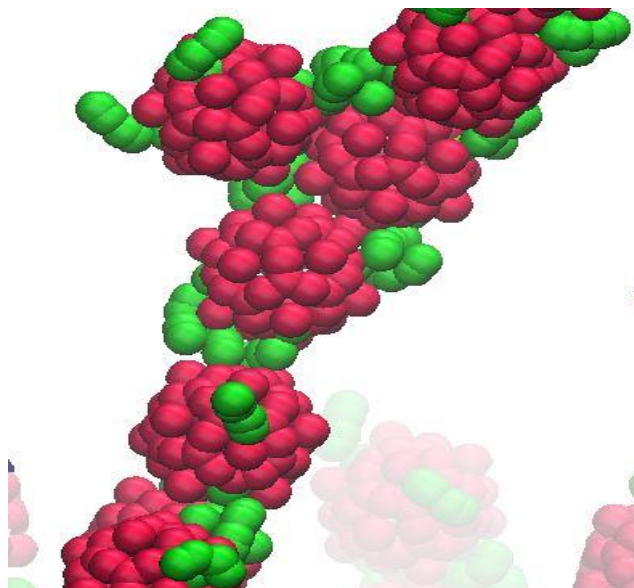
11D) Five chains as in 1F
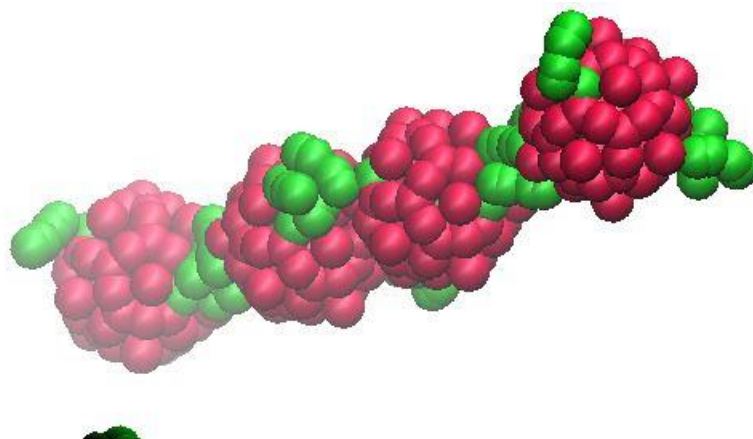
11E) 6 tethers as in 1G
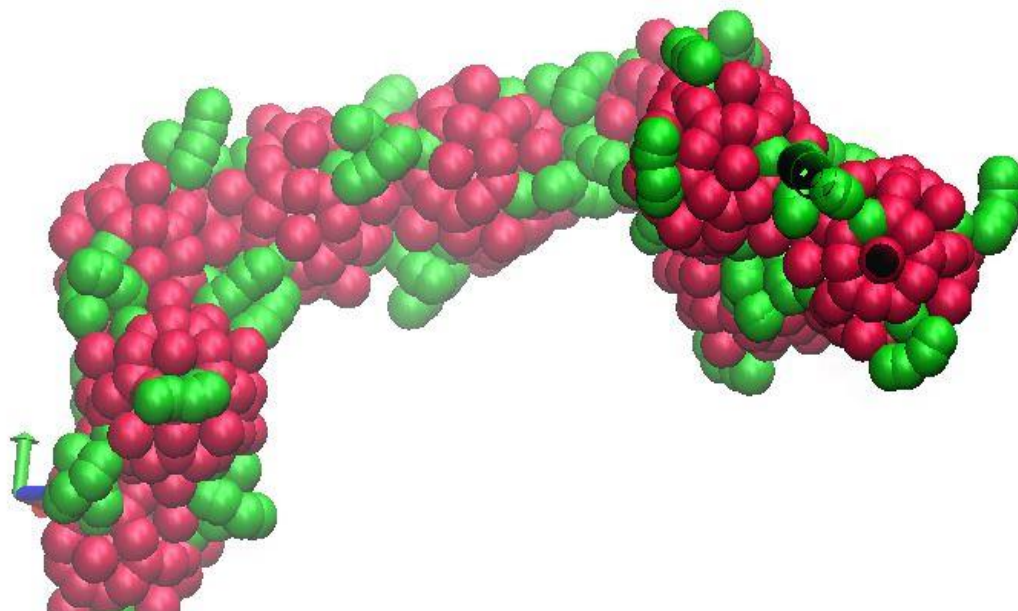
11F) Sheet like pattern formed for 1D , Density = 0.001298, 5beads in tethers, solvent conditions favoring attraction of tethers
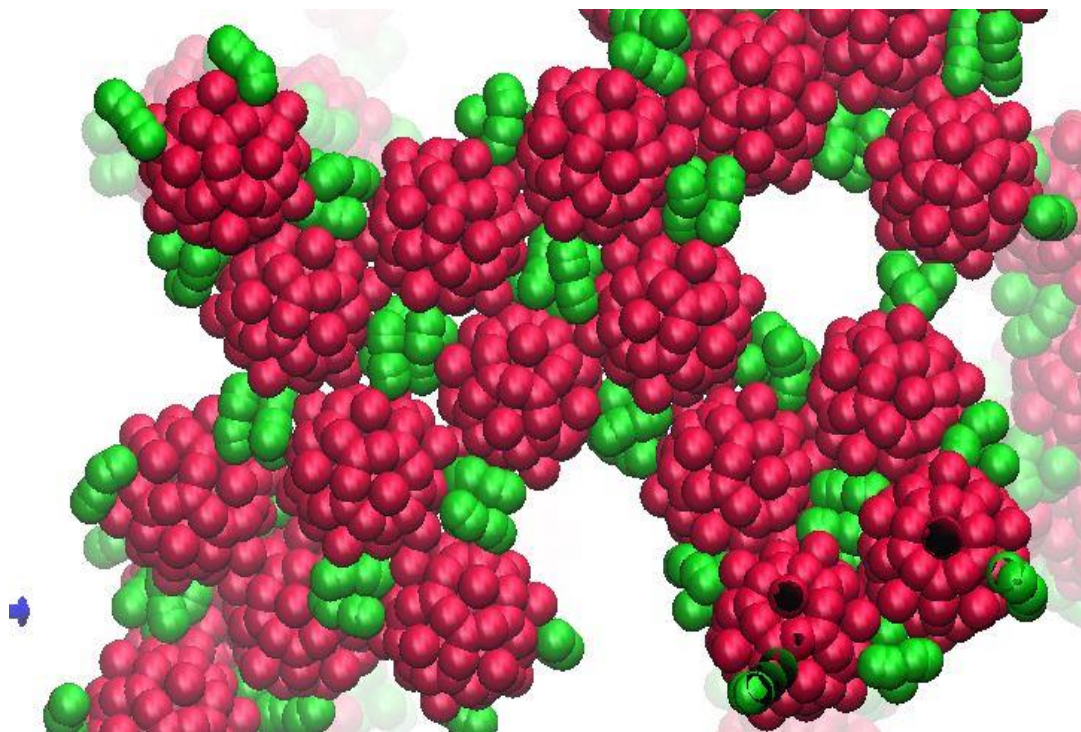
11G) Clustered and Membrane like patterns formed for 6 tether symmetric arrangement as in 1G, Density = 0.001728
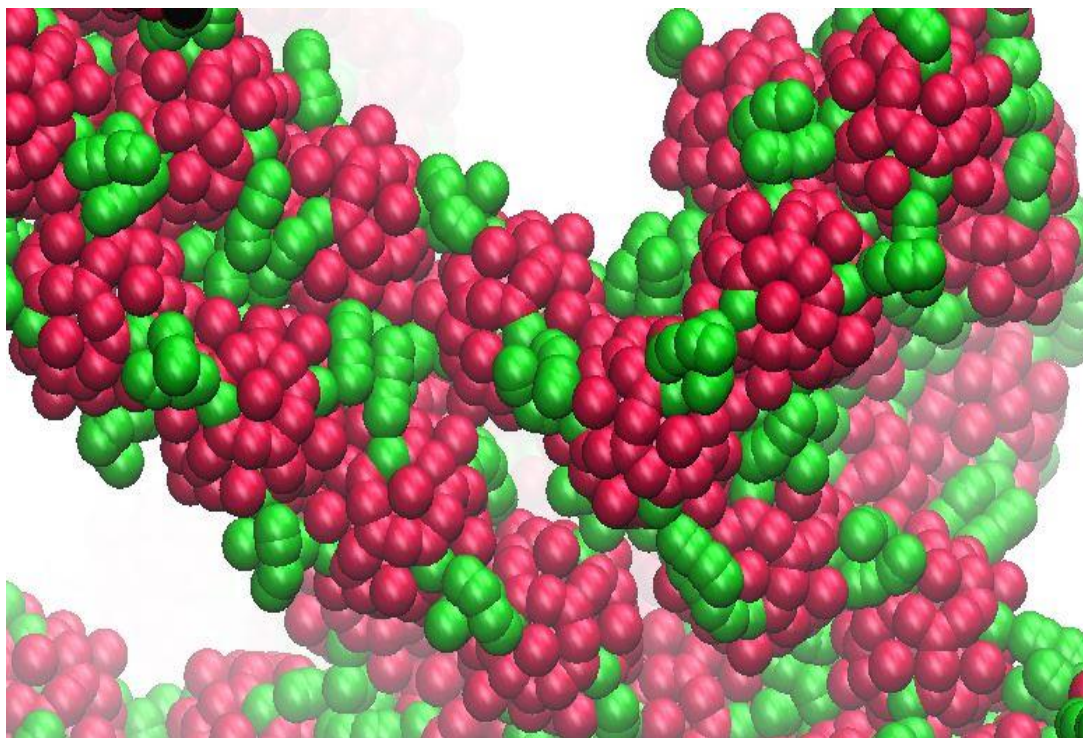
11H) Broken sheets under solvent conditions favoring the attraction of nanoparticle, anisotropy 1G, Density 0.001728
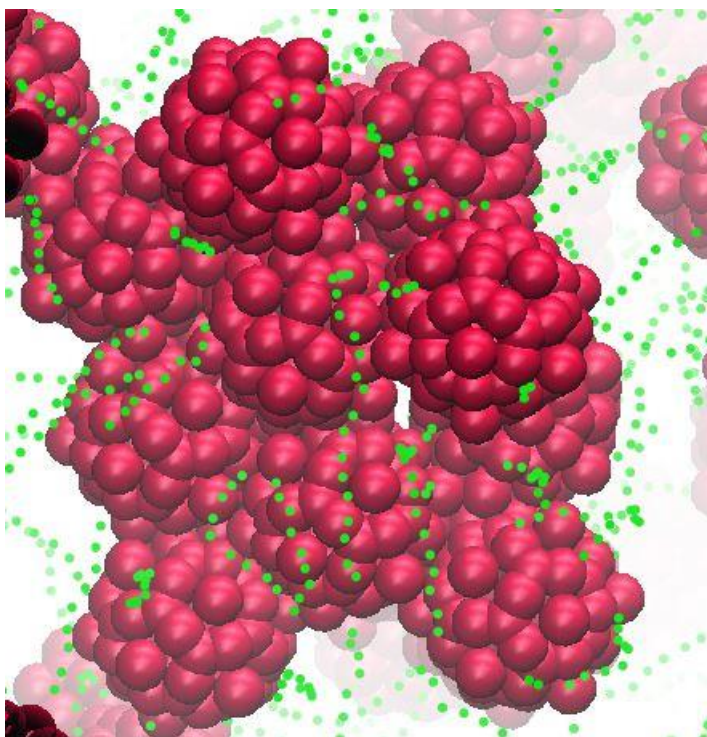
11I) Chains under conditions favoring the attraction of capsids, anisotropy 1D, Density= 0.001728, Number of tether beads = 10.
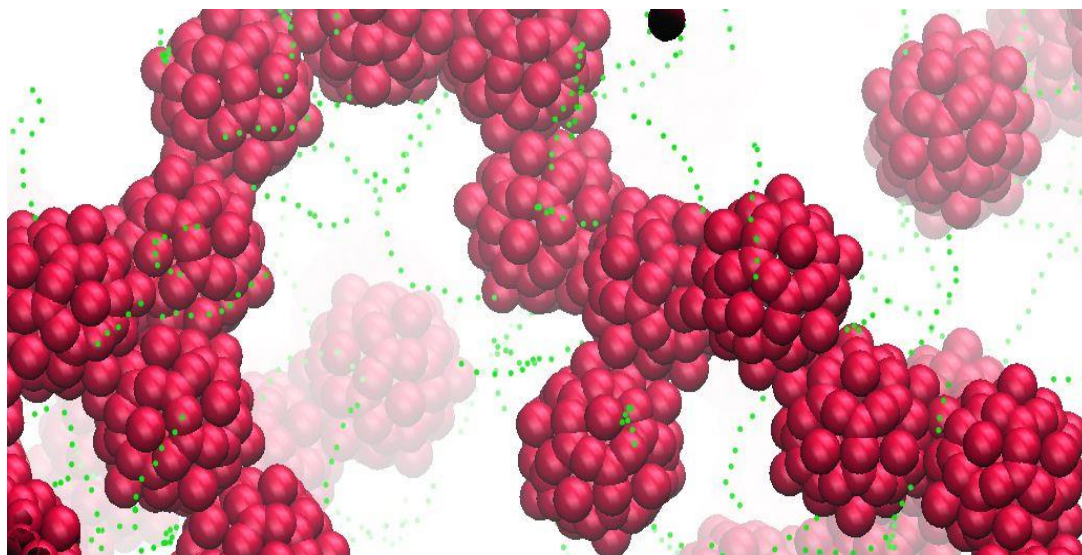
11J) Chains under conditions favoring the attraction of capsids, anisotropy 1E, Density= 0.001728, Number of tether beads = 10.
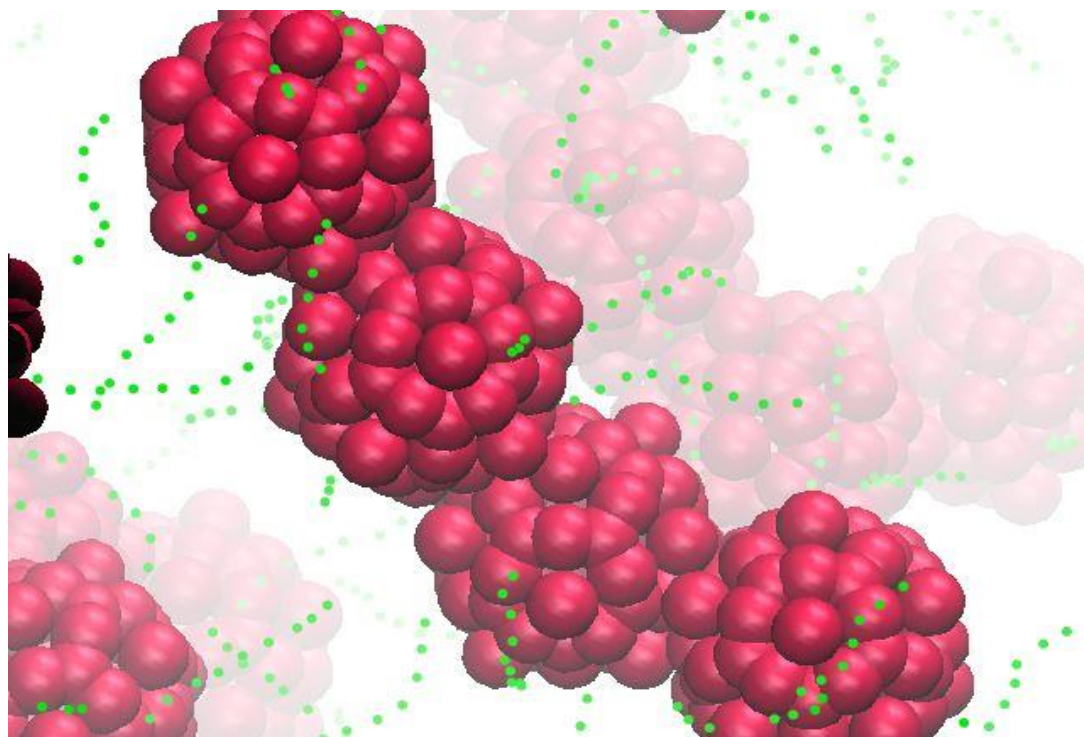
Chapter 4

Conclusions

We have presented, to our knowledge, the first computational simulations for functionalized icosahedral building blocks/coarse grained virus particles, as possible candidates for materials design. This architecture comes up frequently in the synthesis of gold nanocrystals besides the abundant icosahedral virus capsids being investigated for several reasons. This study shows that icosahedral building blocks can form n-mer type aggregates, chains and small 2D patterns. The density region mapped in our simulations predominantly gives chain like arrangements, while 2-D patterns and 3-D random clusters appear rarely, and only towards upper density limits. In the simulations of Bilalbegović [5] similar chain like architectures were obtained. This might indicate a preference of the monomeric icosahedron for forming chain like architectures. Our results indicate that small functional groups (5 beads) direct the assembly better under conditions favoring the aggregation of tethers while small 2-D patterns under solvent conditions favoring the aggregation of nanoparticle, are observed for long tether groups. Also, the number of tethers does not seem to affect the nature of aggregates obtained under the latter solvent conditions within the density region investigated. We have also developed analysis routines for the system giving valuable insights into the final aggregate : Radial Distribution function and Population plot.

The computational materials design approach used in this study can further guide wet lab investigations, and the choice of functionalization for bottom up materials design using these icosahedral building blocks.

Chapter 5

References

(1) Finn, M.G.; Johnson, J.E.; Strable, E. *Nano Lett.* **2004,** *4* (8), 1385-1389.

(2) Lee, W.K.; Cha, S.; Kim, K.; Kim, B.; Lee, *J. Solid State Chem.* **2009**, *182* (12), 3243-3248

(3) Fan, J.A.; He, Y.; Bao, K.; Wu, C.; Bao, J.; Schade, N. B.; Manoharan, V. N.; Shvets, G.; Nordlander, P.; Liu, D. R.; Liu, D. R.; Capasso, F. *Nano Lett.* **2011,** *11*, 4859-4864.

(4) Finn, M.G.; Pokorski, J. K.; Breitenkamp, K.; Liepold, L. O.; Quazi, S. *J. Am. Chem. Soc.* **2011,** *133*, 9242-9245.

(5) Bilalbegović, G. *Comp. Mater. Sci.* **2004,** *31*, 181-186.

(6) Gutiérrez-Sánchez, C.; Pita, M.; Vaz-Domínguez, Shleev, S.; De Lacey, A. L. *J. Am. Chem. Soc.* **2012**, *134*, 17212-17220

(7) Wang, Y.; Wei, G.; Wen, F.; Zhang, X.; Zhang, W.; Shi, L. *J. Mol. Catal*. **2008**, *280* (2), 1-6.

(8) Chang, C.; Yang, K.; Liu, Y.; Hsu, T. *Colloids Surf., B* **2012**, *93*, 169-173.

(9) Avram, M.; Bǎlan, C. M.; Petrescu, I. Schiopu, V.; Mǎrculescu, C.; Avram, A. *Plasmonics.* **2012, 7,** 717-724.

(10) Oh, Ju-Hwan; Lee, Jae-Seung. *Chem. Commun.* **2010,** *46*, 6382-6384.

(11) Leach, A.R. Molecular Modeling Principles and Application, Longman, 1996.

(12) Allen, M.P.; Tildesley, D.J. Computer Simulations of Liquids, Clarendon Press, Oxford, 2001.

(13) Frenkel, D.; and Smit, B. Understanding Molecular Simulation, Second Edition: From Algorithms to Applications, Academic Press, 2001.

(14) Plimpton, S. *J. Comp. Phys*. **1995**, *117*, 1-19*: http://lammps.sandia.gov.*

(15) Tuckerman, M.E.; Berne, B.J.; Martyn, G.J. *J. Chem. Phys.* **1992***, 97(3)*, 1990-2001.

(16) Kendall, E.A. An Introduction To Numerical Analysis, Second Edition, Wiley, 1989.

(17) Carrillo-Tripp, M.; Shepherd, C.M.; Borelli, I.A.; Venkataraman, S.; Lander, G.; Natarajan, P.; Johnson, J.E.; Brooks, C.L. III; Reddy, V.S. *Nucleic Acid Research* **2009,** *37*, D436-D442**.**

(18) Jorgensen, W.L.; Chandrasekhar, J.; Madura, J.D.; Impey, R.W.; Klein. M.L. *J. Chem. Phys.* **1992***, 79(2)*, 1983-1992.

(19) Fennell, C.J.; Gezelter, J.D. *J. Chem. Phys.* **2006**, *124(23)*, 234104-234115.

 (20) Schneider, T.; Stoll, E. *Phys. Rev. B.* **1978**, *17*, 1302-1322.

(21)Dunweg, B.; Paul, W.; *Int. J. Mod Phys. C* **1991,** *2(3)*, 817-827.

(22) Raja, K.S.; Wang, Q.; Finn, M.G. *ChemBioChem* **2003**, 4, 1348-1351.